frontiers in Earth Science

ORIGINAL RESEARCH
published: 25 February 2022
doi: 10.3389/feart.2022.817012

Contained-Reflected Megaturbidites of the Marnoso-arenacea Formation (Contessa Key Bed) and Helminthoid Flysches (Northern Apennines, Italy) and Hecho Group (South-Western Pyrenees)

Roberto Tinterri[1]*, *Tommaso Mazza*[1] and *Pierre Muzzi Magalhaes*[2]

[1]Department of Chemistry, Life Sciences and Environmental Sustainability—Earth Sciences Unit, University of Parma, Parma, Italy, [2]Petrobras (Petroleo Brasileiro), Rio de Janeiro, Brazil

Contained-reflected beds deposited by fully-ponded or partially-reflected turbidity currents are important because their correct evaluation can give important indications on the degree of basin confinement and on the type, size and orientation of the morphological obstacle. Through a detailed facies analysis of various significant megabeds in the Marnoso-arenacea Formation, including the Contessa key bed, in the helminthoid flysches in the northern Apennines (Italy) and in the Pyrenees (megaturbidite MT5), this work proposes a depositional model that is well consistent with the recent experimental data available in the literature, discussing their strengths and limits. The Contessa and flysch megabeds fit very well with the experimental conditions because they are deposited in narrow and elongated confined basins characterized by axial flows. Indeed, in the proposed model, it is possible to recognize facies deposited by: 1) a basal underflow directed towards the bounding slope (Facies A), 2) an intermediate part of the flow characterized by lateral deflections (facies B1), 3) an upper well-developed reversing flow (facies B2) and 4) an uppermost residual reversing flow recording the final collapse of the fine-grained suspended load forming a poorly-sorted slurry facies C and a very thick mudstone unit D. Facies A, B1 and B2 are usually separated by very thin fine-grained muddy drapes rich in carbonaceous matter, which can be traced throughout the basin. These drapes - very common in contained and confined beds in these settings - can be related to internal density surfaces, along which decoupling processes, separating underflows from reversing overflows, can easily occur. Conversely, as the MT5 is characterized by a source transversal to an elongated narrow basin, the large flow volume versus basin capacity hinders the generation of reversing flows and rebound layers favoring the formation of fully-ponded pulsating overflows able to deposit alternations of laminated and massive units. This facies type can be observed in the basins that are characterized by axial flows only near the basin margins where the pulsating collapse of the reversing flow can dominate. This study shows that the integration of detailed field studies are essential to validate experimental data from an applicative point of view.

Keywords: megaturbidites, contained-reflected beds, facies analyses, contessa megabed, helminthoid flysches

OPEN ACCESS

Edited by:
Rosanna Maniscalco, University of Catania, Italy

Reviewed by:
Salvatore Milli, Sapienza University of Rome, Italy
Giacomo Dalla Valle, National Research Council (CNR), Italy

***Correspondence:**
Roberto Tinterri
roberto.tinterri@unipr.it

Specialty section:
This article was submitted to Sedimentology, Stratigraphy and Diagenesis, a section of the journal Frontiers in Earth Science

Received: *17 November 2021*
Accepted: *14 January 2022*
Published: *25 February 2022*

Citation:
Tinterri R, Mazza T and Magalhaes PM (2022) Contained-Reflected Megaturbidites of the Marnoso-arenacea Formation (Contessa Key Bed) and Helminthoid Flysches (Northern Apennines, Italy) and Hecho Group (South-Western Pyrenees). Front. Earth Sci. 10:817012. doi: 10.3389/feart.2022.817012

1 INTRODUCTION

Contained-reflected beds deposited by fully (ponded) or partly reflected turbidity currents have long been studied with experimental works, numerical modeling and facies analysis. They are very important because the correct evaluation of the flow reflection nature and direction can give important indications not only on the degree of basin confinement but also on the type, size and orientation of morphological obstacles, which, in foreland basins, are generally tectonic structures (e.g., Kneller, 1995).

In spite of the various depositional models based on field data (Pickering and Hiscott, 1985; Haughton, 1994; Remacha et al., 2005; Tinterri and Muzzi Magalhaes, 2011; Bell et al., 2018) and recent experimental and numerical models that have tried to clarify the dynamics of reflected to fully-ponded turbidity currents (Patacci et al., 2015; Howlett et al., 2019; Soutter et al., 2021), the processes and resulting facies of these types of contained-reflected flows are still poorly understood in detail and various problems remain open. First of all, a detailed depositional model aimed at recognizing the various experimental phases in ancient turbidites is not yet well defined. Secondly, other more specific open problems are the distinction between combined flow structures and mud-controlled sedimentary bedforms (e.g., Tinterri, 2011; Baker and Baas, 2020), as well as the interaction between flow reflections and the formation of mud-rich transitional flows able to deposit poorly-sorted slurry facies (e.g., Tinterri et al., 2016; Bell et al., 2018). Contained-reflected beds can be found in all depositional elements of a turbidite system but ponded beds deposited by low-density turbidity currents dominate especially the basin plains or lobe fringes where the interaction between flow decelerations and dynamics of mud rich transient turbulent flows (*sensu* Baas et al., 2011) can become important.

This work wants to present several recorded cases of bed types and facies tracts of megaturbidites deposited by high- and low-density turbidity currents related to flow reflections perpendicular and oblique to the morphology in partially or fully confined settings. These examples mainly come from turbidites in the northern Apennines (Marnoso-arenacea Formation, MAF and helminthoid flysches, i.e., M. Cassio and Solignano Formations), and in the southern Pyrenees (megaturbidite MT5 in the Banaston turbidite system). All these deposits are suitable for discussion of open problems and try to propose depositional models that can link experimental and field data. In particular, this objective is achieved through a detailed physical stratigraphy and facies analysis of the Contessa key bed, i.e., the main key bed of the MAF (e.g., Ricci Lucchi and Valmori, 1980; Muzzi Magalhaes and Tinterri, 2010).

2 PREVIOUS WORKS: LABORATORY EXPERIMENTS AND DEPOSITIONAL MODELS

When a turbidity current encounters a topography, the flow can be laterally deflected or completely reflected, depending on the obstacle size in relation to the flow volume, the geometry of the slope and the angle of incidence of the current (Tinterri, 2011; Patacci et al., 2015). In this case the flow can be defined as "confined" if the confining topography partially or totally traps the current, and, in case of total entrapment, the turbidity current can be also defined as "contained". Consequently, the confined and contained turbidity currents can be also defined as ponded turbidity currents in which a flat-topped suspension cloud is established (Patacci et al., 2015).

The first laboratory experiments available in the literature focused on the processes related to lateral (Kneller et al., 1991; Haughton, 1994; Amy et al., 2004) and frontal rebounds (e.g., Pantin and Ledeer, 1987; Alexander and Morris, 1994; Edwards et al., 1994) of surge type flows discussing especially the dynamics of internal waves propagation. However, as Kneller and Branney (1995) and Kneller (1995) introduced a model that was based on various combinations of different spatial and temporal accelerations (i.e., nonuniformity and unsteadiness, respectively) and was able to produce markedly different vertical and lateral variations in the resulting turbidite bed, they highlighted, for the first time ever, the importance of submarine topography in controlling flow deflection and reflection, as well as variations in flow velocity in space (flow nonuniformity) producing anomalous intrabed vertical sequences, multiple current directions and locally enhanced deposition.

Conversely, the recent experiments by Patacci et al. (2015) focused on the behavior of sustained ponded suspension clouds showing that ponded flows are characterized by a well-determined sequence of dynamic phases. More precisely, a flow impinging a confining slope produces, firstly, a flow reversal causing a bore or soliton up current propagation that leads to an initial inflation phase of ponded suspension. Then, the progressive flow inflation forms a circulation of a ponded suspension characterized by an underflow directed towards the bounding slope and an upper return layer separated by a well-developed internal density and velocity interface where internal waves can propagate. Finally, cloud deflation on waning of input produces final settling of fines from a static cloud (**Figure 1A**).

More recently, numerical experiments by Howlett et al. (2019) have given results similar to those obtained by Patacci et al. (2015). These models discuss turbidity currents impinging against a topography perpendicular to the flow direction, and highlight that a supercritical current decelerated and thickened due to the hydraulic jump on the counter-slope, where a reverse overflow formed through current self-reflection and a reverse underflow was issued by backward squeezing of a dense near-bed sediment load (see **Figure 1B**). Very similar results can be also observed in the works by Woods et al. (1998), Lamb et al. (2004), Lamb and Parsons (2005), and Toniolo et al. (2006). The experimental results by Howlett et al., 2019 have been further investigated by Soutter et al. (2021), studying, in addition to a morphology perpendicular to the incoming flow, cases in which the topography is parallel and oblique to the flow.

Conversely, the sedimentary structures indicating flow reflections and ponding processes are relatively well established in the literature thanks especially to the depositional models by Pickering and Hiscott (1985) from the Cloridorme Formation, by Haughton (1994) from the Sorbas basin, Remacha et al. (2005) from the Hecho basin and Tinterri and Muzzi Magalhaes (2011) from the MAF (see **Figures 1D,E**).

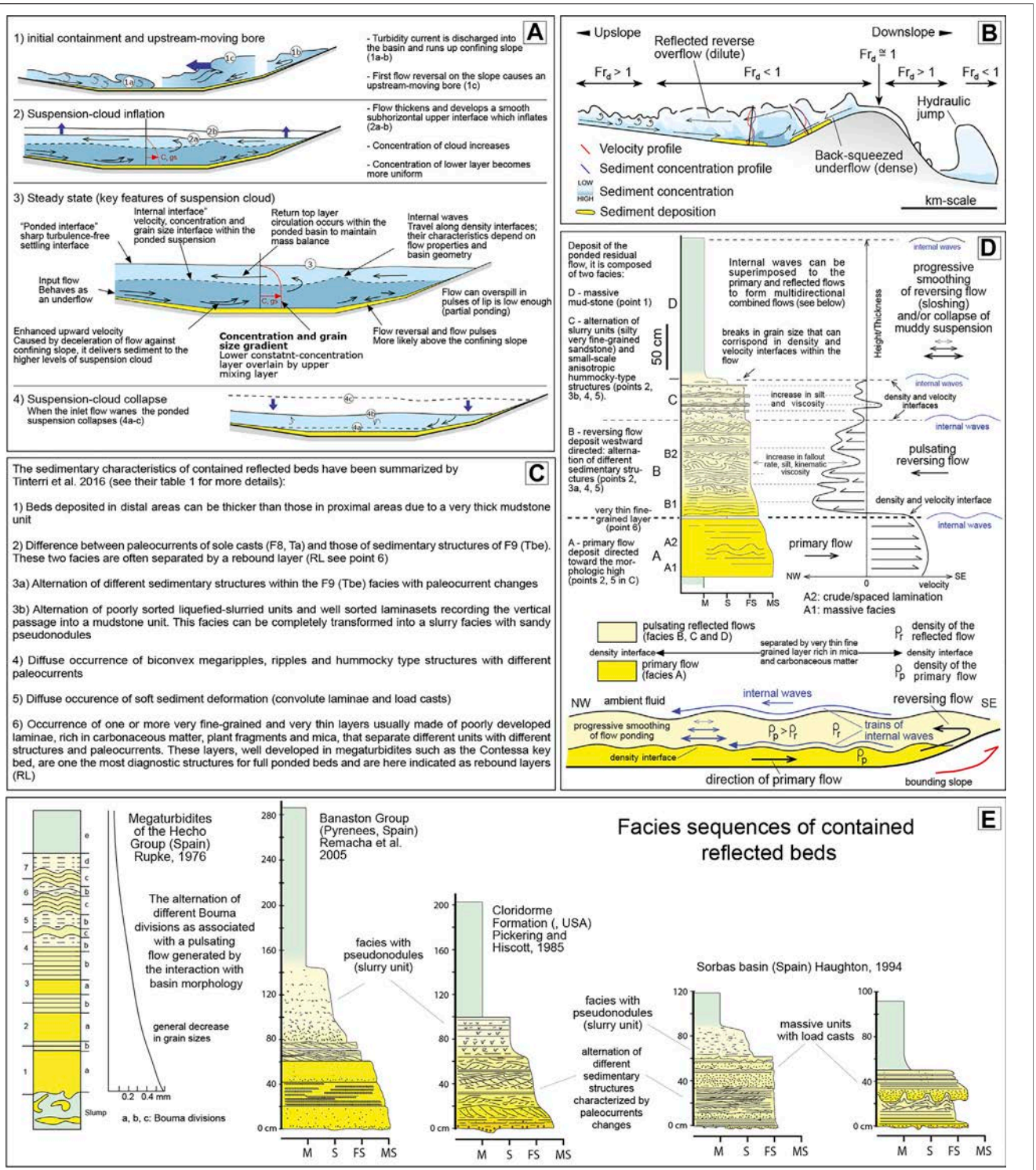

FIGURE 1 | (A) Scheme of a ponded suspension cloud from laboratory experiments by Patacci et al. (2015), **(B)** Schematic diagram summarizing the flow reflection dynamics against a morphologic obstacle (from Howlett et al., 2019), **(C)** List of the main diagnostic sedimentary structures characterizing contained-reflected beds (from Tinterri et al., 2016), **(D)** Model describing a frontal reflection, which tries to link the facies sequence of a typical contained-reflected bed in the Marnoso-arenacea Formation with the dynamics of a pulsating reflected turbidity current (from Tinterri et al., 2016); **(E)** Main facies sequences of contained-reflected beds discussed in the literature [see also **(D)**].

In particular, Tinterri et al., 2016 proposed a depositional model based on the studies carried out over the last 10 years in the MAF, trying to summarize the main sedimentary characteristics of the contained-reflected beds in basin plain (**Figures 1C,D**). These sedimentary structures, which are summarized in **Figure 1C**, can characterize both fully contained ponded beds and not-contained strata that undergo only lateral and frontal rebound.

Furthermore, the dynamic behavior of the turbidity currents in a confined basin changes according to flow concentration (high- and low-density) and to the degree of flow-density stratification that can favor hydraulic jumps and decoupling processes (see Postma et al., 2009; Postma and Cartigny, 2014; Tinterri et al., 2016). For these reason, facies and processes of high and low-density flows in fully-ponded basins, mainly characterized by frontal reflections, will be discussed with the aim to try to show new facies models and a possible link with the available experimental data.

3 FULLY CONTAINED AND CONFINED "PONDED" MEGATURBIDITES

These bed types can be seen as contained-reflected beds in which the degree of basin confinement versus the flow volume allows fully-ponded conditions. The turbidity currents that deposit these types of beds are able to cross the entire basin and to undergo one or more reflections. In general, these bed types can be seen as megaturbidites, i.e., very thick beds of virtually basin wide extent that usually form excellent key beds (see Mutti et al., 1984). Magnificent examples of megaturbidites are those in the south western Pyrenean foreland basin, where each megaturbidite consists of a bipartite graded bed up to 200 m thick displaying a basal megabreccia that contains large slabs of shallow water limestones and outsize rip-up marlstone clasts, which pass upward into an up to 20 m graded unit composed of a basal coarse-to fine-grained biocalcarenite characterized by an alternations of horizontal and ripple lamination (Rupke, 1976; see **Figure 1E** and below) and an upper homogeneous calcareous mudstone (see Labaume et al., 1983; Labaume et al., 1987; Mutti et al., 1999; Payros et al., 1999). These megaturbidites can be interpreted as deposited by bipartite flows composed by a basal dense flow and an upper turbulent flow produced by the evolution and transformation of fast-moving, inertia-driven avalanche-blocky flows (*sensu* Ogata et al., 2012) derived from adjacent carbonate platforms triggered by major seismic shocks associated with thrust propagation. On the basis of the sedimentary structures described by Rupke (1976), it can be inferred that the upper turbulent flow must have undergone important reflections and rebound processes as occurred in other megaturbidites, such as the Gordo bed in the Sorbas basin (Kleverlaan, 1987) and Megabeds of the Cervarola Sandstones (Tinterri and Piazza, 2019; Piazza and Tinterri, 2020) and in the Cerro Bola Fm. in Argentina (Falgatter et al., 2016). Other famous examples come from the Eocene flysch of the Dalmatia in Croatia (Marjanac, 1990). Consequently, the upper graded beds characterizing these bipartite megaturbidites are the most likely to present the characteristics of ponded beds.

The Contessa key bed in the MAF, the megabeds of the Helminthoid flysches (northern Apennines, Italy) can represent very good examples of these bed types characterizing the upper part of the megaturbidites and deposited by turbulent flows as in the case of the megabed at the top of MT5 (Hecho Group). In particular, being characterized by a massive to crudely laminated coarse-grained basal unit, the Contessa key bed and MT5 megabed can be interpreted as deposited by high-density turbidity currents, whereas the megabeds of the Cassio Fm., being characterized by fine-grained laminated basal sandstone, can be interpreted as deposited by a low-density turbidity current.

3.1 The Contessa Key Bed (Marnoso-arenacea Formation)

3.1.1 Introduction

The Contessa Key bed (CKB, Renzi, 1964; Ricci Lucchi and Pialli, 1973; Ricci Lucchi and Valmori, 1980) is the most important key bed in the MAF foredeep turbidites (Langhian-Tortonian) in the northern Apennines (Italy), (**Figure 2A**). The MAF turbidites, deposited in an elongate, NW-stretched foredeep basin formed in front of the growing Northern Apennines orogenic wedge, were fed mainly by Alpine sources to the north, whereas minor sources providing hybrid and carbonate sediments included shallower water carbonate platforms along the southern and south-eastern margins of the basin (Gandolfi et al., 1983; Ricci Lucchi, 1986). The main sediment dispersal pattern was longitudinal and the northwest to southeast flowing turbidity currents had a siliciclastic composition. By contrast, carbonate and hybrid turbidites flowing in the opposite direction, i.e., towards the north-west, produced the main key beds (**Figure 2A**). Together with the fact that, among foredeep turbidites, the MAF is the best exposed and less structurally deformed one due to its relatively external position within the Apenninic orogen, these marker beds have favoured detailed physical stratigraphy studies, such as the pioneering one by Ricci Lucchi and Valmori (1980) and more recently those by Amy and Talling (2006) and Muzzi Magalhaes and Tinterri (2010) and Tinterri and Tagliaferri (2015), (see also Tagliaferri and Tinterri, 2016; Tagliaferri et al., 2018).

Thanks to the regional stratigraphic framework by Muzzi Magalhaes and Tinterri (2010), (see **Figures 2B,C**), it can be stated that the Contessa key bed is located in a stratigraphic interval characterized by tectonic quiescence allowing this megabed to be traced in the entire basin, i.e., over an area of about 125 × 25 km (Ricci Lucchi and Valmori, 1980; Muzzi Magalhaes and Tinterri, 2010).

3.1.2 Description

The high-resolution stratigraphic framework of the CKB has been carried out through the measurement and description of 23 stratigraphic logs parallel and perpendicular to the paleocurrents directed towards the northwest (**Figures 2D**, **3A**, **4**; see also Tinterri and Mazza, 2019).

In general, the CKB, with thickness ranging from 9 to 15 m, is a normally graded bed characterized by a well-developed bipartition highlighted by a basal sandstone unit ranging from 3.5 to 6.5 m and an upper mudstone unit with thickness ranging from 5 to 9 m (**Figure 2E**). The basal sandstone unit is characterized by high

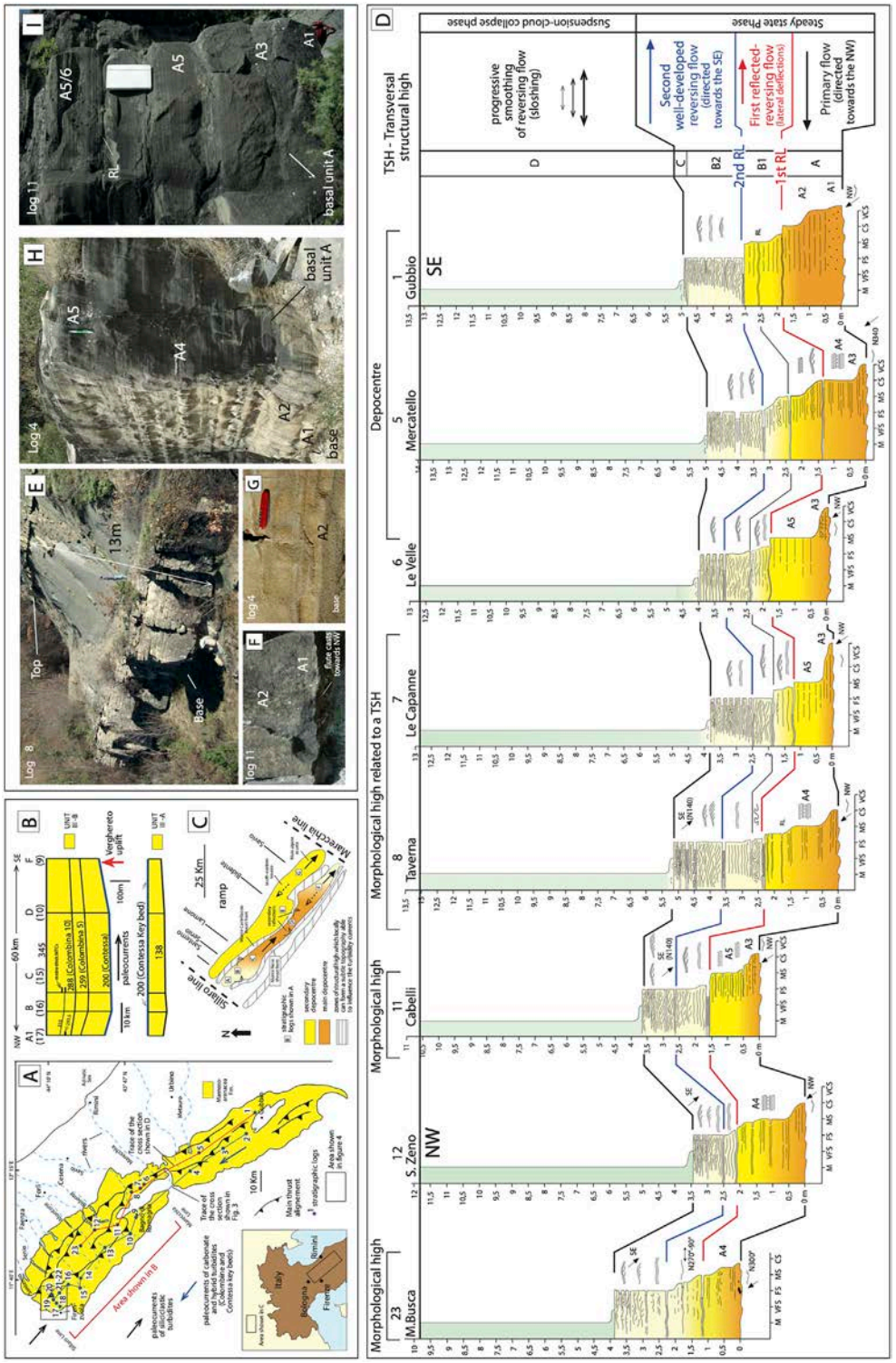

FIGURE 2 | (A) The MAF cropping out in the Northern Apennines, with the locations of the Contessa key bed stratigraphic logs, **(B)** Stratigraphic-cross section of the MAF Unit III including the Contessa key bed (from Muzzi Magalhaes and Tinterri, 2010), **(C)** Schematic paleogeography of the basin during the deposition of Unit III (from Tinterri and Muzzi Magalhaes, 2011), **(D)** Detailed stratigraphic cross section of the Contessa megabed in the outer basin (see red trace in **Figure 2A**). On the right the interpretation in terms of facies and processes is shown. The flow phases on the right are those by Patacci et al. (2015); **(E)** Contessa megabed in Log 8; **(F,G)** Details of basal coarse-grained massive facies A1 and crudely laminated facies A2 (logs 11 and 4, respectively); **(H)** Facies characterizing the basal part of the CKB deposited by the primary flow (Log 4); **(I)** Details on the basal part of the CKB below the first rebound layer (1st RL) deposited by the primary flow (Log 11). For the location of stratigraphic logs, see **(A)**.

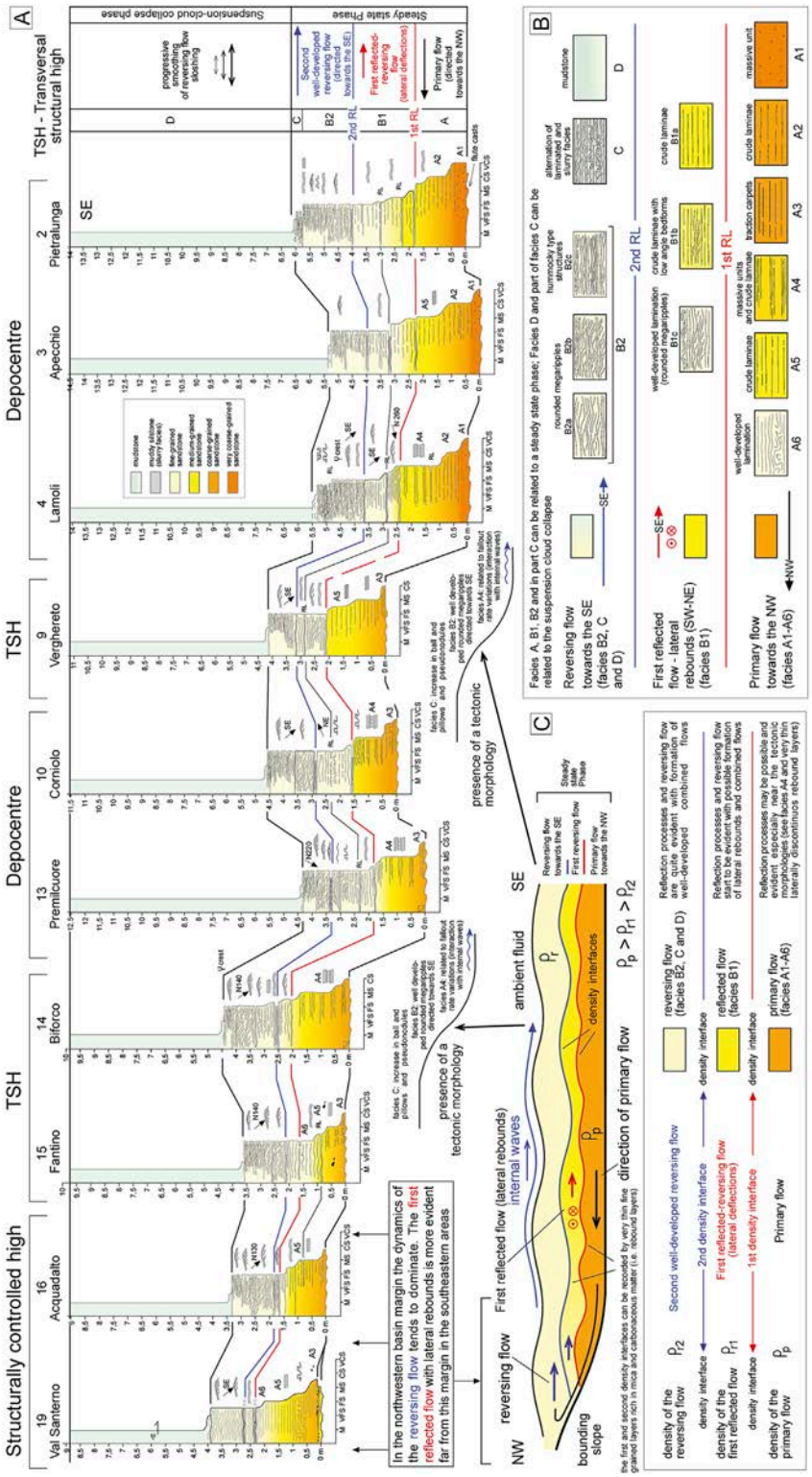

FIGURE 3 | (A) Detailed stratigraphic cross section of the Contessa megabed in the inner basin (see blue trace in **Figure 2A**). On the right, the interpretation in terms of facies and processes is also shown. The flow phases on the right are from Patacci et al. (2015); **(B)** Facies scheme of the CKB with facies deposited by the primary flow, first reflected flow characterized by lateral deflections and reversing flow; **(C)** Depositional model of the CKB.

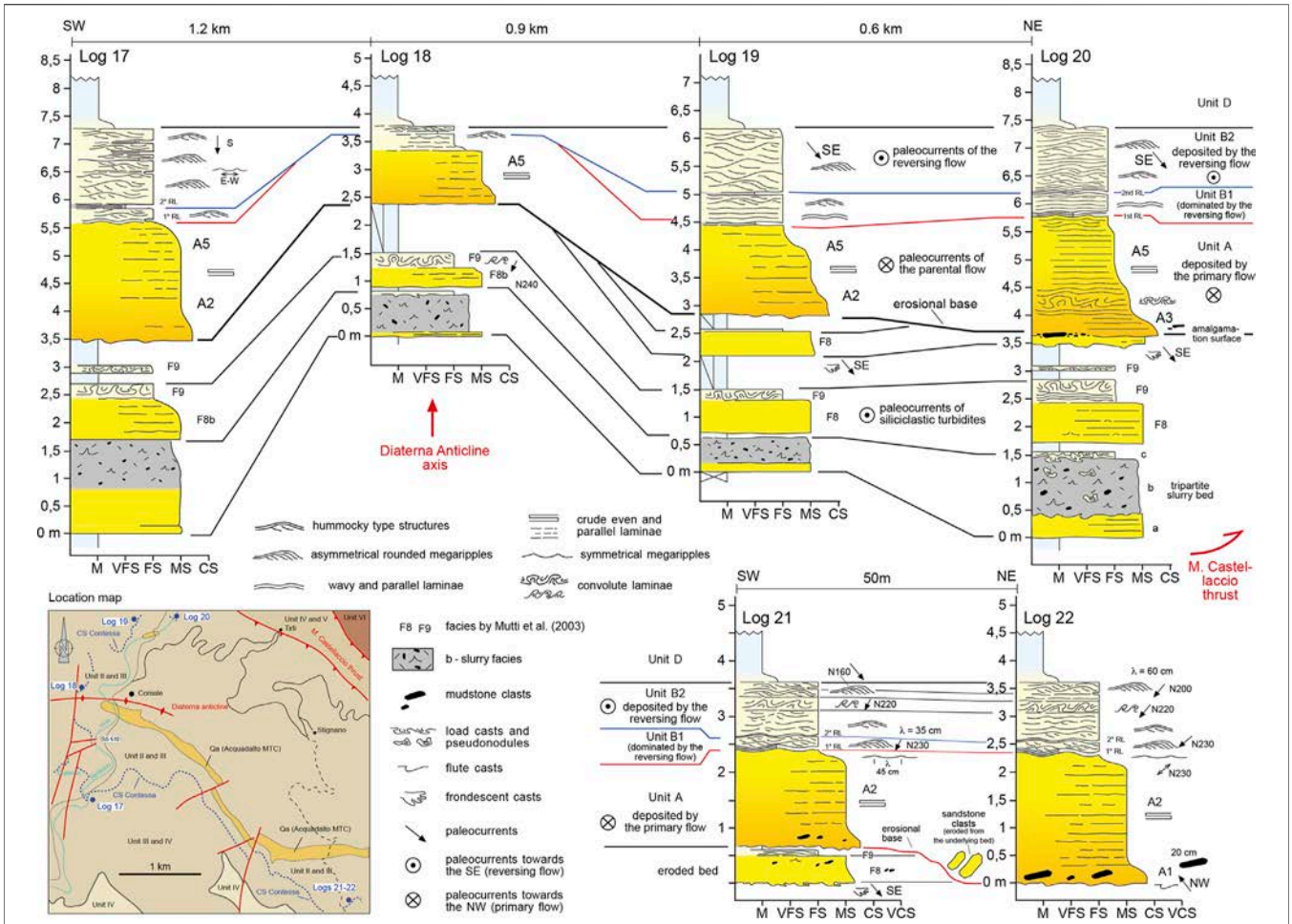

FIGURE 4 | Stratigraphic cross section of the CKB in the Santerno Valley. It is perpendicular to the main structural alignments and the paleocurrent of the primary flow directed towards the NW. It is to be noted the stratigraphic pinchings and the erosional capacity of the CKB controlled by the Diaterna anticline axis and M. Castellaccio thrust (see **Figure 2A** for the position of the location map, see also de Jager, 1979).

variability in term of grain sizes, sedimentary structures and paleocurrents; however, the occurrence of two evident very thin and fine-grained layers rich in carbonaceous matter and plant fragments (i.e., the rebound layers RL by Tinterri et al., 2016) allow the sandy part of the CKB to be distinguished in three intervals, namely basal, intermediate and upper (see **Figures 2D**, **3**; see also Tinterri et al., 2019b). In particular, **Supplementary Table S1** in the supplementary materials shows the list of the facies introduced in this work and their comparison to the facies scheme by Mutti et al. (2003).

The basal one is made of granular very coarse-to medium-grained sandstone characterized by well-developed flute casts indicating paleocurrents towards the northwest. On the basis of the grain sizes and sedimentary structures in this basal interval, at least six facies can be distinguished, which, from the coarsest to the finest ones, are: A1) massive granular very coarse-grained sandstone (**Figures 2F–I**). This facies can be found in the more proximal logs 1, 2, 3 and 4 (see **Figures 2D**, **3A**) and can also be associated with mudstone and sandstone intraclasts, sand injections and delamination structures characterized by vertical erosional surfaces (**Figure 4**; see also Felletti et al., 2019); A2) crude laminated very coarse to coarse-grained sandstones (**Figures 2G,H**, **3**); A3) coarse-grained sandstone characterized by a well-developed traction carpets; A4) coarse to medium-grained sandstone characterized by an alternation of crudely laminated and massive units. This facies can be found especially in the intermediate logs 4, 8, 10, 13 and 14 (**Figures 2H**, **3**); A5) crudely laminated medium-grained sandstones; A6) laminated fine-grained sandstone. Facies A5 and A6 are found especially in the more distal logs 16 and 19 (**Figures 3**, **4**).

In general, facies A1 tends to evolve into facies A5 and A6, through intermediate facies A2, A3 and A4, both downcurrent and upward within the basal unit. The latter, mainly composed of facies A1-5, is separated from the intermediate unit by a first very thin and fine-grained layer (i.e., a rebound layer-RL). This thin layer can be traced relatively well in the entire study area (see 1st RL—red fine-grained drape in **Figures 2D**, **3A**, **5**) and is highlighted by the widespread occurrence of carbonaceous matter and plant fragments (**Figures 5D,E**).

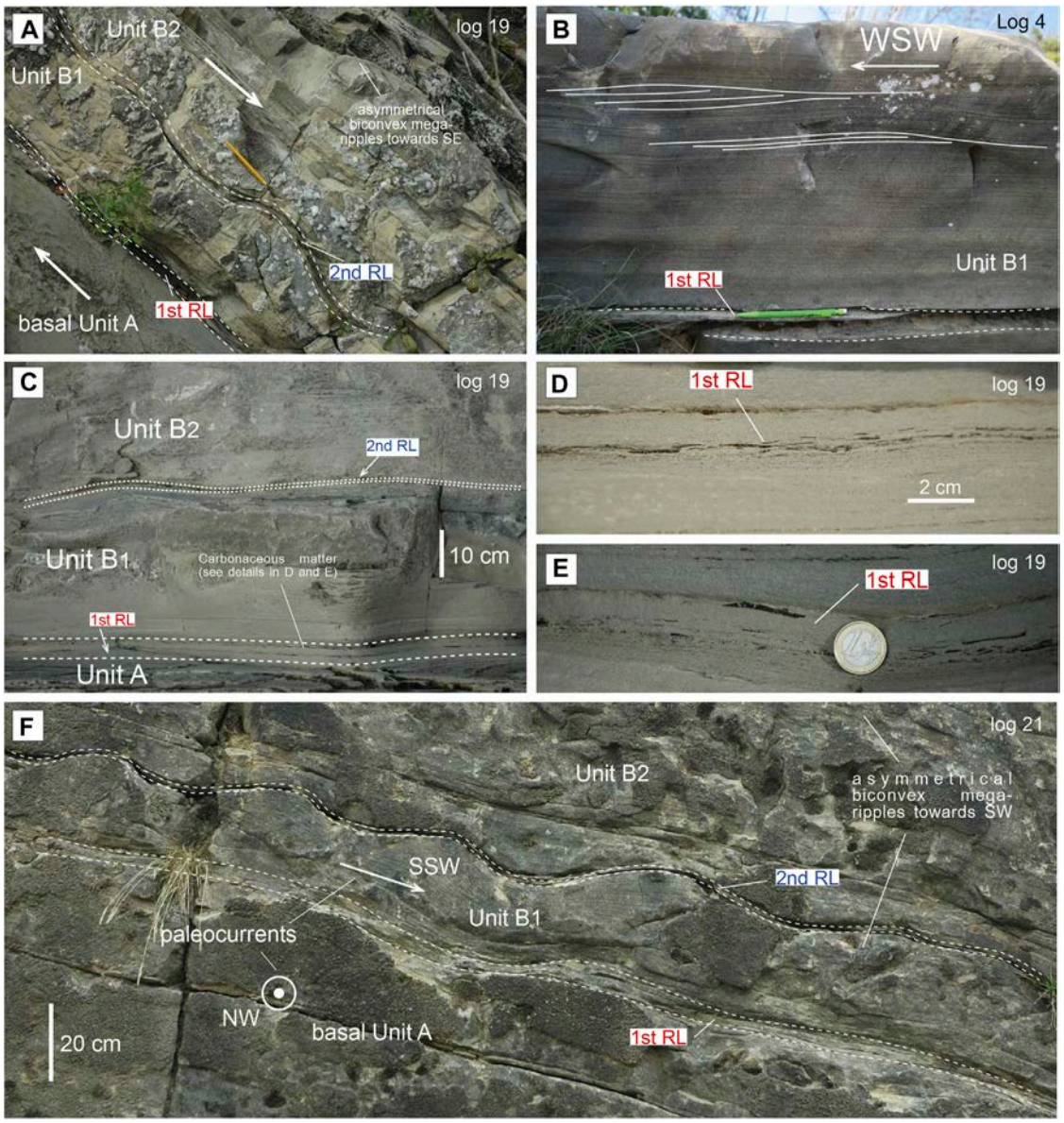

FIGURE 5 | (A) Examples of facies B1 and B2 in Log 19 (Santerno valley) separated by the 1st (red) and 2nd (blue) evident rebound layers; **(B)** Facies B1 in Log 4 (Lamoli) with evidence of lateral deflections; **(C)** Facies B1 and B2 separated by the 1st (red) and 2nd (blue) rebound layers in Log 19; **(D,E)** First rebound layer separating facies A and B rich in carbonaceous matter (see C for the location of the photos); **(F)** Facies B1 and B2 separated by the 1st (red) and 2nd (blue) rebound layers (Log 21); to be noted the slightly asymmetrical megaripples with paleocurrents towards the SW in Unit B1 (see **Figure 4** for the location of the Logs).

The intermediate unit B1 is made of, at least, three facies (see **Figure 3**, **Supplementary Table S1**), namely: B1a) medium to fine-grained sandstone characterized by crude even and parallel lamination that sometimes shows subtle undulations or very low-angle laminae. This facies occurs especially in more proximal southern logs 1, 2 and 3 (see **Figures 2**, **3**); B1b) similar to B1a, this facies is characterized by the appearance of anisotropic hummocky-like megaripples (wavelength of about 30–40 cm) showing paleocurrents roughly perpendicular to or at high angle with those indicated by the flute casts directed towards northwest (see log 4, **Figures 3**, **5B,C**); B1c) fine-grained sandstone characterized by a poorly-developed alternation of crude even/undulated and parallel lamination with hummocky-type megaripples showing paleocurrents directed towards the southeast, i.e., in the opposite direction vs. the north-westward paleocurrents indicated by flute casts (**Figures 5A,F**). In general, facies B1a tends to evolve into facies B1c, in a downcurrent direction, even if the appearance of the hummocky megaripples seems to be related to specific basin morphologies (see **Figures 2D**, **3**).

The intermediate sandstone unit is separated from the upper sandstone unit by a second very thin and fine-grained layer,

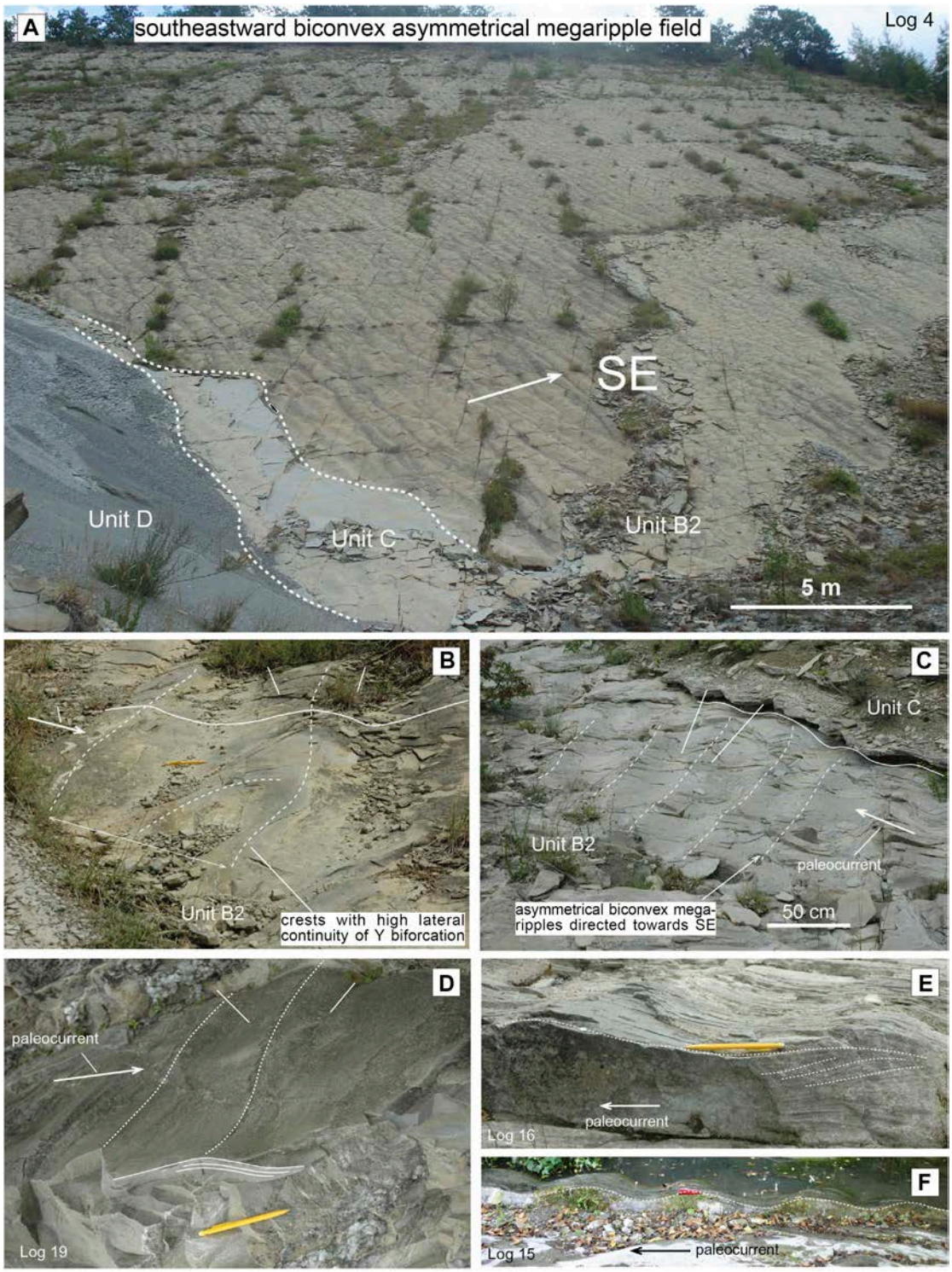

FIGURE 6 | (A) Spectacular and famous outcrop near Lamoli (Log 4) showing a field of south-eastward biconvex megaripples, where the large lateral continuity of the crests can be also observed. These megaripples characterize Unit B2 and are deposited by a well-developed reversing flow (see **Figure 3C** for the interpretation); **(B)** Biconvex megaripples characterized by a typical Y bifurcation (Log 14); **(C)** Asymmetrical biconvex megaripples with a high-lateral continuity of the crests (Taverna near Log 8); **(D–F)** Examples of biconvex (rounded) megaripples with sigmoidal-cross laminae in Logs 19, 16 and 15, respectively. See **Figures 2A,D**, **3A** for the location of the logs.

which, as the first, can be traced relatively well in the entire study area (see 2nd RL—blue fine-grained drape in **Figures 2**, **3**, **5**). This layer is also characterized by widespread occurrence of carbonaceous matter and plant fragments.

The third upper sandstone unit is composed of two main facies indicated as B2 and C in **Figures 2D**, **3**, **6** and **Supplementary Table S1**. Facies B2 is made of fine to very fine-grained sandstone and is characterized by widespread occurrence of biconvex asymmetrical megaripples always indicating paleocurrents directed towards the southeast, i.e. in the opposite direction vs. the north-westward paleocurrents indicated by flute casts. These megaripples have a wavelength of about 40–50 cm and are characterized by internal sigmoidal-cross laminae (**Figure 6**). The crests have high lateral continuity (**Figures 6A–F**) showing sometimes well-developed Y bifurcations very similar to those of wave ripples (**Figure 6B**).

Facies B2 can be subdivided into three different categories (see **Figure 3**, **Supplementary Table S1**), namely: 1) facies B2a entirely composed of the biconvex asymmetrical megaripples described above, 2) facies B2b characterized by an alternation of undulated laminae and symmetrical biconvex megaripples and hummocky-type structures and 3) facies B2c mainly composed of wavy to even and convolute laminations. Facies B2a tend to evolve towards the south into facies B2c, i.e. in the same direction indicated by the biconvex megaripples. The megaripples of facies B2a are consistent with the reversing or back flow ripples by Parea and Ricci Lucchi, 1975 (see also Ricci Lucchi and Valmori, 1980; Ellis, 1982; Ricci Lucchi, 1995).

Facies B2 pass upward into facies C, which records the vertical transition to the upper mudstone unit D. Facies C is made of an alternation of poorly-sorted silty to muddy very fine-grained slurried sandstone and well-developed laminasets generally characterized by anisotropic hummocky-type megaripples directed towards the south-east and widespread soft-sediment deformation represented by convolute laminae and load casts. The latter are represented by ball and pillows characterizing the base of the laminasets, which can evolve in detached pseudonodules within the underlying poorly-sorted slurried facies. Facies C is not present everywhere but only in well-determined zones that generally are associated to structural highs (see logs 4, 6, 7 and 8 in **Figure 3A**).

Facies C records the vertical passage into the uppermost facies D composed of a very thick mudstone unit characterized by an apparently massive facies (**Figure 3**).

As mentioned above, the CKB is deposited in the stratigraphic Unit III by Muzzi Magalhaes and Tinterri (2010) and, although this is a unit deposited during a period of relatively tectonic quiescence, the increase and decrease in the CKB thickness tend to be consistent with the depocentres and structural highs highlighted the high-resolution stratigraphic framework carried out by Muzzi Magalhaes and Tinterri (2010). Mudstone and sandstone intraclasts in facies A and erosive delamination structures tend to be located in those logs in which a stratigraphic pinching can be observed (see **Figures 2D**, **4**). Generally, these stratigraphic pinchings are located near tectonic structures as showed by the stratigraphic-cross section of **Figure 4** where erosional features and the lowest thickness in the CKB are located above the Diaterna anticline axis.

3.1.3 Interpretation

Based on the facies descriptions the CKB can be interpreted as a typical contained and reflected bed in which the degree of basin confinement allows fully-ponded conditions (see Parea and Ricci Lucchi, 1975; Ellis, 1982; Ricci Lucchi, 1995; Tinterri and Muzzi Magalhaes, 2009, Tinterri and Muzzi Magalhaes, 2011). Indeed, facies A, B, C and D are consistent with the facies categories introduced by Tinterri et al. (2016) for contained-reflected beds (see also Tinterri et al., 2012; Tinterri et al., 2019b). However, thanks to the detailed facies analysis of the CKB, a detailed depositional model can be advanced in which the two very fine-grained layers that can be interpreted as rebound drapes (RL; see Tinterri et al., 2016; Tinterri et al., 2019a), play a key role.

The basal sandstone unit of the CKB can be divided into three units (A, B and C) thanks to two main fine-grained very thin levels rich in carbonaceous matter (1st and 2nd rebound drapes, see **Figure 3** and **Supplementary Table S1**). The first one (red line) separates the basal facies A deposited by a high-density primary flow (directed towards the NW) from the intermediate unit composed of facies B1 in which sedimentary structures indicating lateral reflections and reversing flow start to be common. Conversely, the second RL (blue line) separates the intermediate unit from the upper sandstone unit dominated by biconvex asymmetrical megaripples and hummocky-type structures (facies B2 and C) indicating paleocurrents directed towards the SE and produced by a well-developed reversing flow directed towards the same direction, i.e., SE. These very thin rebound drapes must record a deposition from a relatively quiescent period after reflected or reversing flows had bypassed.

As well known in the literature, the CKB, characterized by a hybrid composition (Gandolfi et al., 1983), was deposited by a turbidity current coming from the south. The source area, able to supply terrigenous and intrabasinal sediment, is thought to be located in a southeastern area of the Apenninic margin (Gandolfi et al., 1983). Consequently, facies A1 to A6 were deposited by the basal part of a bipartite flow represented by a high-density primary flow evolving towards the northwest. This flow can be highly erosive as testified by well-developed bulbous flute casts and delamination structures able to erode the underlying beds (see also Felletti et al., 2019). In this case, in the basal facies A1, mudstone and sandstone clasts can be common (see Log. 15 in **Figure 3A** and **Figure 4**). Delaminations structures, however, seem to be associated with tectonically-controlled basin morphologies that can enhance flow impacts and erosive processes (see **Figure 4**). Log 15 is associated with the Val Lamone tectonic structure separating an uplifted northwestern area from a depocentral southeastern zone (see Muzzi Magalhaes and Tinterri, 2010) whereas the stratigraphic cross section in **Figure 4**, perpendicular to the paleocurrents and to the Diaterna anticline axis and M. Castellaccio thrust shows that these structures can enhance the erosive capacity of the flows and bed amalgamations (see Log 19).

In particular, massive facies A1 is interpreted as deposited by high rates of fallout able to suppress the turbulence at the boundary layer, whereas facies A3, dominated by traction carpets, can be seen as a traction-dominated facies recording the bypass of a sandy high-density turbidity current able to transport northwards the medium-grained sand that would then form the depositional crudely laminated facies A4 and A5 (see **Supplementary Table S1**). The crude or spaced lamination indicates progressive aggradation under a high rate of fallout forming a near-bed suspension in which well-developed tractive structures are prevented by the absence of a sharp rheological interface between the lowest parts of the flow and the just-formed deposit (Kneller and Branney, 1995). In particular, the alternation of crude laminations and massive units characterizing facies A4 may be interpreted as related to decreases and increases in fallout rates generated by increases and decreases, respectively, in flow velocity and turbulence energy. These types of variations can be induced by constructive and destructive interferences between internal wave trains, produced by lateral reflections against the basin margins, and the unidirectional turbidity current directed towards the north (Tinterri, 2011; Patel et al., 2021). Indeed, facies A4 is well developed to the south of the following tectonic structures: Verghereto (Log 4), Lamone (Logs 13, 14, 15) and Diaterna anticline (Logs 21, 22) (see **Figures 3A**, **4**).

The basal unit A is separated from the upper unit B1 by the first RL, which can be deposited by the tail rich in carbonaceous matter and mica of the upper turbulent flow bypassing the deposits of unit A. This bypass can be induced by lateral flow reflections rather than a well-developed reversing flow, since no well-developed reversing megaripples directed towards the southwest are present. These lateral rebounds and decelerations of the bipartite flow can favor decoupling processes with the detachment and partial bypass of the upper turbulent flow (see **Section 6.1** for more details). Indeed, in the second sandstone unit B1, facies B1a tends to decrease in thickness towards the northeast, passing into facies B1c through facies B1b in which megaripples directed towards northeast and southwest, i.e., roughly perpendicular to the primary flow, are common. The reversing megaripples directed towards the south start to be present especially in distal zones, i.e., in Logs 14, 17, 21 (**Figures 3A**, **4**) and this can be associated with the beginning of a complete reflection of the upper turbulent flow favoured by the presence of important transversal tectonic structures, such as those of the Sillaro and Val Lamone lines (see Tinterri et al., 2019a, **Figure 3A**). According to the stratigraphic framework by Muzzi Magalhaes and Tinterri (2010), in the northwestern area, the stratigraphic unit III including the CKB is deposited in a tectonically uplifted zone as testified by the stratigraphic pinching of this unit towards the northwest and the occurrence of large-volume mass-transport deposits (see **Figures 2A–C**). In particular, the area of the Lamone valley (Logs 14, 15, **Figure 3A**) separates a northwestern uplifted area from a southeastern depocenter located in the Bidente valley (see Log 10); it is here supposed that this zone may be associated to a transversal tectonic structure related to the Sillaro line that could produce a barrier able to induce complete reflection of a turbidity current coming from the south, as also supposed by Ellis (1982). Consequently, in distal areas near the northern basin margin, facies B1 passes into a thin B1c facies testifying that the flow is dominated by processes related to the reversing flow (see **Figure 3**).

The evidence of a clear reversing overflow directed towards the southeast is present in the upper sandstone units B2 and C where well-developed biconvex megaripples and anisotropic hummocky-type structures can be found (see **Figure 6**). In general, climbing-biconvex megaripples with sigmoidal-cross laminae (facies B2a) pass downcurrent (i.e., towards the southeast) into symmetrical small-scale hummocky-type structures and wavy to even laminae (facies B2c) suggesting a south-eastward evolution of the reversing flow.

These megaripples have been interpreted as traction-plus-fallout structures related to a unidirectional backflow (Parea and Ricci Lucchi, 1975; Ricci Lucchi and Valmori, 1980; Ellis, 1982), or as antidunes by Ricci Lucchi (1985) and more recently as supercritical dunes propagating in the same direction of the backflow (see Fedele et al., 2016). These megaripples, however, are very similar to the biconvex megaripples reproduced in laboratory under combined flows dominated by unidirectional components (see Yokokawa, 1995; Dumas et al., 2005; Tinterri, 2011). This evidence suggests that they can be deposited by asymmetrical combined flows in which also the fallout rate must play an important role (e.g. Tinterri, 2011).

These structures can be evidence of an interaction between a unidirectional turbidity current and an oscillatory component associated with different trains of internal waves produced by reflection processes. These internal waves propagating along the internal density surfaces can be characterized by very complex interferences resulting from the overlapping of different wave trains able to produce high-velocity multidirectional combined flows, which are at the base of hummocky-type structures. The downcurrent passage from biconvex megaripples into isotropic hummocky structures and low-angle wavy to even laminae can be related to progressive deceleration of the reversing flow that favor the progressive increase in the fallout rate and traction-plus-fallout processes. This, together with a multidirectional oscillatory component, hinder the development of flow separations on the lee side and relative vortices, preventing the formation of regular bedforms (ripples and dunes) and favoring plane beds or quasi-planar laminations which, draping low-angle erosive surfaces, can produce hummocky-type structures (Tinterri, 2011). The long straight crests of the megaripples characterized by large lateral continuity and by Y bifurcations, typical of wave ripples (**Figure 6D**), suggest that the oscillatory component had to be important, reinforcing the interpretation of current-dominated combined flow structures (see Harms, 1969; Tinterri, 2011).

The interpretation of a reversing flow explains very well the second rebound drape separating the upper facies B2 by the underlying intermediate facies B1. Indeed, it is interpreted to be deposited by a diluted tail of the upper turbulent flow bypassed towards the northwest. Undergoing a reflection produced by a northern basin margin, this flow can form a reversing flow directed towards the southeast, able to deposit the megaripples of facies B2 (see **Section 6.1**).

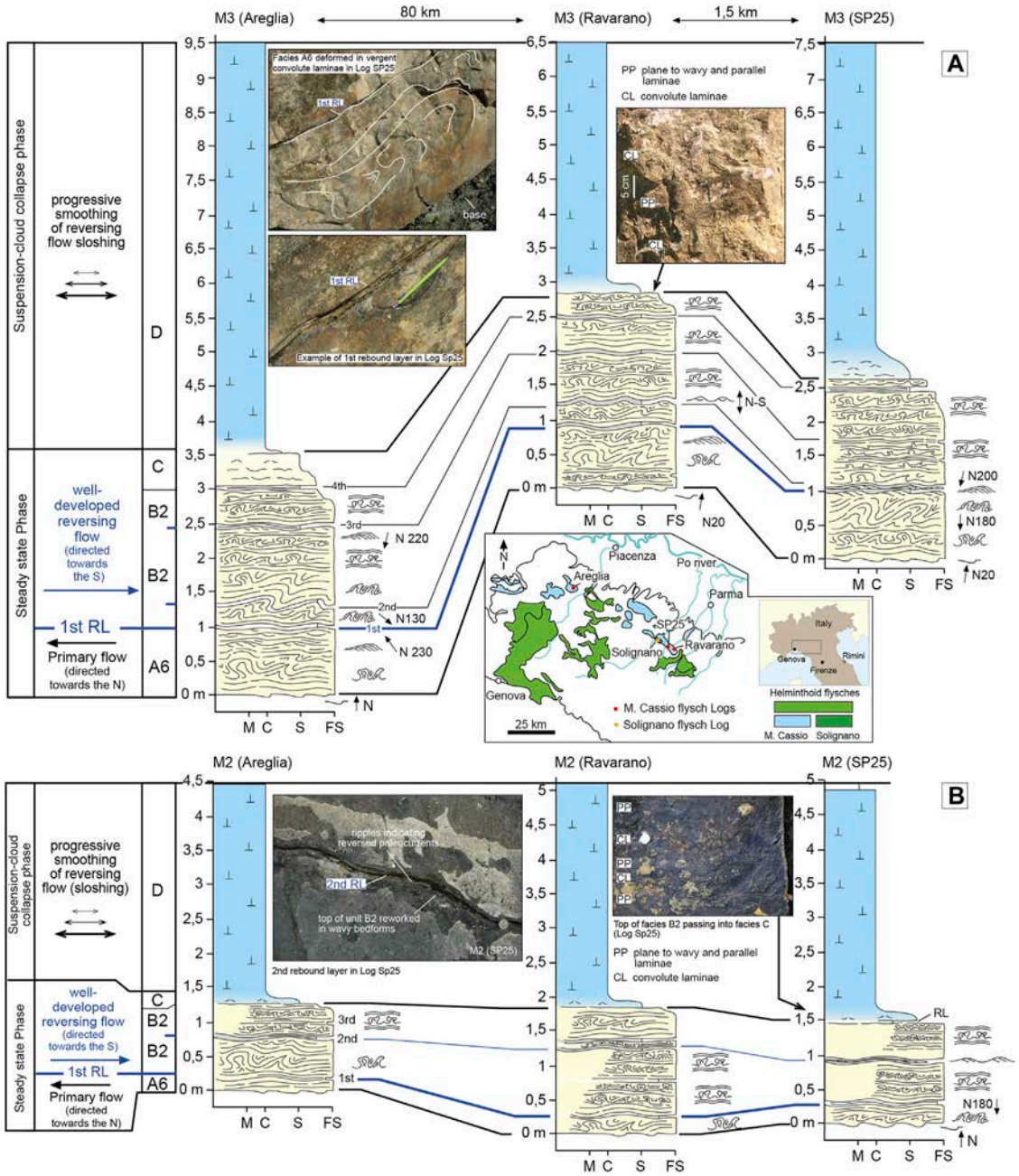

FIGURE 7 | (A) Stratigraphic cross section of megabed M3. Details of the 1st RL, of vergent convolute laminae in facies A6 and the alternations of plane-parallel and convolute laminae at the top of Unit B2 are also shown. A location map of the stratigraphic logs is also shown; **(B)** Stratigraphic cross section of megabed M2, details of the 2nd RL and alternations of plane-parallel and convolute laminae at the top of facies B2 are also shown (see **Supplementary Figure S1** in the supplementary materials for more details).

Facies B2 passes upward into facies C characterized by an alternation of poorly-sorted slurried units and well-sorted laminasets. This facies is very common in contained-reflected beds, and can be interpreted as deriving from an interaction of collapse of final suspension cloud (see Patacci et al., 2015), cyclic-wave loading of reflected flows (testified by the combined flow structures and the changes in paleocurrents, Tinterri et al., 2016) and the dynamics of the silty and muddy grain sizes (see Baas et al., 2011; Baker and Baas, 2020). This facies records the passage to the upper very thick mudstone unit D in its turn recording the deposition of the residual muddy turbulent flow.

In conclusion, the CKB depositional model may be consistent with the steady state phase 3 and suspension-cloud collapse phase 4 of the experimental model proposed by Patacci et al. (2015) (see

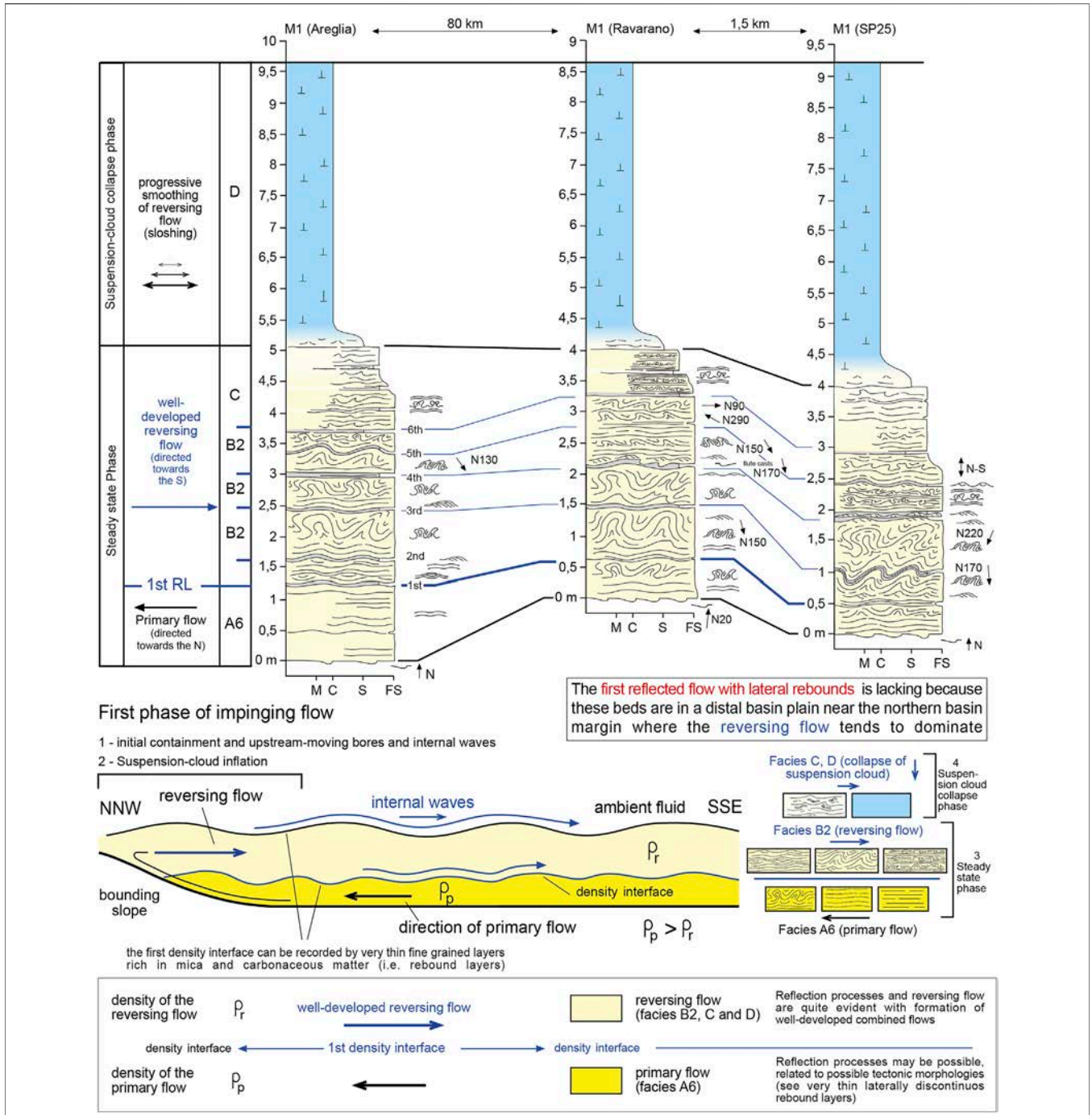

FIGURE 8 | Stratigraphic cross section of megabed M1. Below, facies scheme and depositional model of the M. Cassio Flysch megabeds are also shown (compare to CKB depositional model in **Figure 3C**).

Figure 1A), where two main rebound drapes (1st and 2nd RLs) recording two density interfaces, allow to subdivide the turbidity current, able to deposit the CKB, into three parts (see **Figure 3** and **Supplementary Table S1**): I) a first basal high-density primary flow deriving from to the south and that decelerates towards the north (Facies A), II) a second more diluted turbulent upper part that, although still related to a flow coming from to the south, starts to record lateral rebound processes, and, in more distal zones (i.e., the north western areas), the first evidence of reversing flow (Facies B1c) and III) a third uppermost more diluted turbulent flow that records a well-developed reversing flow that, after the reflection against a northern morphological barrier, evolves towards the south east (Facies B2 and partially C; **Figure 3**). The final deposition

of the mud (Facies D) can be related to the deflation of a steady cloud characterizing the entire basin even if an interaction with sloshing internal waves cannot be completely ruled out as testified by the thickness variations consistent with the basin morphology controlled by the main tectonic structures. This interaction can also enhance decelerations and suspension-cloud collapses that can contribute to the formation of slurry facies C (**Figure 3**).

3.2 The M. Cassio Flysch Megabeds: Fully-Contained (Ponded) Beds

3.2.1 Introduction

The Monte Cassio Flysch (MCF) is composed of deep water turbidites that belong to the External Ligurian Units in the Northern Apennines (Italy) and mark, together with the other Upper Cretaceous helminthoid flysches, the beginning of the Tethys Ocean closure and, consequently, of the alpine orogenesis (Vescovi et al., 1999; Marroni et al., 2001). The MCF thickness, more than 1800 m, consists of basin plain siliciclastic, carbonate and mixed turbidites of the Late Campanian age (Rio e Villa, 1987), deposited in a narrow and elongate basin below the CCD (Scholle, 1971; Sagri e Marri, 1980; Baruffini and Papani, 2017; Marroni et al., 2017). The MCF stratigraphic succession consists of beds whose composition indicates mixing of sediments derived from intrabasinal and terrigenous sources; some of these beds are megabeds characterized by a graded laminated hybrid sandstone passing upward into a very thick marlstone. The biogenic particles that characterize these megabeds range from fine-grained sand (fragments of echinoderms and bryozoans, benthic and planktonic foraminifera, fine pelecypods, sponge spicules, calcareous algae) to mud (coccoliths and fine spicules) (see Zuffa et al., 2004).

3.2.2 Descriptions

The MCF stratigraphic succession is characterized by more than twenty megabeds that represent regional key beds; however, a detailed facies analysis of three of these megabeds (i.e., beds M1, M2 and M3 in **Supplementary Figure S1**) highlights facies sequences very similar to that of CKB. Megabeds M1, M2 and M3 are consistent with beds 1,040, 1,080 and 1,100 by Baruffini and Papani (2017) and, thanks to the high-resolution stratigraphic framework performed by Mazza and Tinterri (in preparation), these beds can be traced for about 100 km (**Figure 7A**, see also Baruffini and Papani, 2017). These correlations show that these beds are characterized by a basal fine-grained sandstone with well-developed laminations that pass upward into a very thick marlstone.

In all studied beds, the basal sandstone units are characterized by a well-developed alternation of different types of sedimentary structures, such as wavy to even and parallel laminae, hummocky-type structures, convolute laminations with different degrees of vergence and ripples (**Figure 7**). Vergent convolute laminae, anisotropic hummocky structures and ripples show different paleocurrents from those of flute casts indicating flows towards the north.

In particular, as for the CKB, the presence of various fine-grained drapes (i.e., rebound layers) allows the basal sandstone units to be divided into different facies that show these paleocurrent changes.

The first fine-grained drape (1st blue line in **Figures 7**, **8**) divides a basal laminaset generally composed of even to wavy and parallel laminae with flute casts indicating paleocurrents towards the north-northeast (facies A6) from upper laminasets dominated by ripples and vergent convolute laminae showing paleocurrents in the opposite direction (i.e. towards the south-southwest, see facies B2 in **Figures 7A**, **8** and **Supplementary Table S1**). In particular, in its upper part, facies A can already show vergent convolute laminae and ripples indicating paleocurrent towards the south (**Figures 7**, **8**).

Facies B2 is made of various laminasets separated by fine-grained drapes that are characterized by various very peculiar structures, such as large-scale hummocky geometries, very thin laminates made of ripples, deformations associated with vergent convolutes. In some cases, flute casts at the base of B2 laminasets indicating paleocurrents in the opposite direction vs. the flute casts of facies A6, are found (see the 2nd drapes in the bed M1 at the Log Ravarano, **Figure 8** and **Supplementary Figure S1E**).

The vertical passage to the marlstone unit D is recorded by facies C made of silty very fine-grained sandstone and is characterized by widespread soft-sediment deformations consisting of convolute laminae, ball-and-pillows and pseudonodules. In some cases, however, in facies C, well-developed alternations of even to wavy and parallel laminae, low-angle bedforms and small-scale convolute laminae can be recognized (see bed M1 in the Ravarano Log, **Figure 8**). This evidence suggests that a continuum between these two facies types can exist.

Finally, Facies D is composed of a very thick marlstone, which generally has thickness similar or higher than that of the basal sandstone unit. This unit apparently shows a massive facies, although very thick faint laminations can be observed.

3.2.3 Interpretations

Facies descriptions allow the MCF megabeds to be interpreted as typical confined and contained beds, in which the degree of basin confinement allows fully-ponded conditions. Facies A, B, C and D, as for CKB, are perfectly consistent with the facies categories introduced by Tinterri et al. (2016), and the fine-grained and very-thin drapes can be interpreted as rebound layers recording a deposition during a relatively quiescent period occurring after the bypass of reflected or reversing flows (see **Section 6.1**, Tinterri et al., 2016). They highlight the three facies, A, B and C, of the basal sandstone unit (see **Figures 7**, **8** and **Supplementary Table S1**).

In particular, the first rebound drape (1st blue line in **Figures 7**, **8**) separates the basal facies A, which can be interpreted as deposited by a low-density primary turbidity current directed towards the N from an upper unit deposited by a reversing flow represented by a low-density turbidity current flowing in the opposite direction. This is testified by ripples, vergent convolute laminae and anisotropic hummocky-type structures indicating paleocurrents towards the S. The basal facies A in comparison to those of the CKB is dominated by A6, since it represents a more

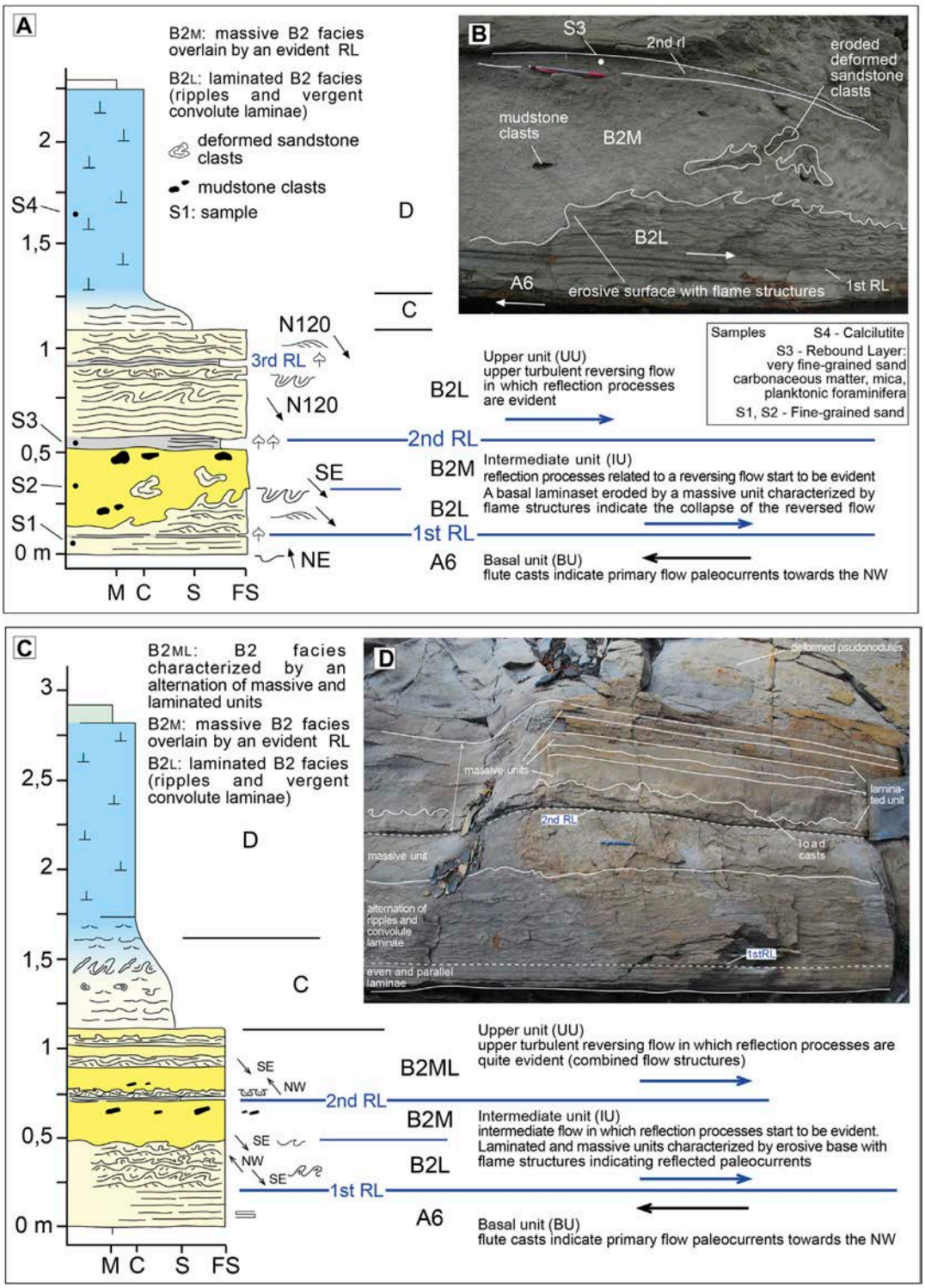

FIGURE 9 | (A) Description and interpretation of a megabed in the Solignano Flysch characterized by massive units with an erosional base and flame structures. The location of the samples used for the grain-size analysis is also shown; **(B)** Detail of massive facies B2M characterized by folded mudstone and sandstone clasts, erosional base and flame structures (see Log in A); **(C)** Description and interpretation of another megabed in the Solignano Flysch characterized by massive units with an erosional base and load structures. These bed types have been interpreted as indicating proximity to the bounding slope; **(D)** Megabed shown in C in which the main facies are also indicated (see **Supplementary Figures S2, S3** in the supplementary materials for more details). See **Figure 7A** for the beds location.

distal facies than the A5 facies in CKB (**Figures 4**, **8**; see **Supplementary Table S1**). From this point of view, the megabeds of the MCF may be seen as a downcurrent evolution of beds showing a facies sequence similar to that of the CKB.

However, unlike the CKB, the MCF megabeds do not seem to be characterized by the intermediate facies B1 with lateral deflections. Conversely, the basal facies A6 is directly overlain by facies B2 indicating a well-developed reversing flow. This evidence may be explained by the fact that these beds represent a downcurrent evolution of megabeds similar to the CKB suffering more from the effects of frontal reflections with development of a reversing flow.

The laminasets of facies B2 are generally separated by various rebound layers that are generally less developed than those associated with the reversing flow (**Figures 7A**, **8** and **Supplementary Figure S1**). A possible explanation is that the reversing flow can undergo various minor lateral reflections sufficient to produce a delay in the lateral bores allowing the formation of fine-grained rebound layers. In this case reversing flows can propagate in a unsteady pulsating way, i.e., through low-frequency reversing surges where the tail of every surge has the time to deposit an RL through a mechanism similar to that described by Kane et al. (2009), (see **Section 6.1** for more details; see also Patel et al., 2021). Indeed, a pulsating reversing flow can be considered the rule in ponded confined basins, where the interaction with lateral rebounds due to basin margins or uneven (bumpy) intrabasinal morphologies can produce complex flow velocity variations at different frequency and scales (see Tinterri, 2011; see also; Patacci et al., 2015; Howlett et al., 2019). At large-scale, low-frequency pulsating reversing surges can play an important role in the deposition of the rebound layers, whereas, at small-scale, multidirectional combined flows can be related to an interaction between pulsating reversing flows and different trains of internal waves due to multiple lateral rebounds (Tinterri, 2011).

From this point of view, the formation of alternations of different structures, such as convolute and plane to wavy parallel laminae, can be related to these flow velocity variations (see **Figure 7A**), while symmetrical ripples with a dominant trochoidal geometry and low-angle hummocky-type structures having different degree of anisotropy show that an oscillatory component must be present within the flow, supporting the interpretation of multidirectional-combined flows (**Figures 7A**, **8**). However, in the formation of low amplitude hummocky-type structures, the dynamics of mud and silt at the boundary layer in transient turbulent flows should also be taken into account (see Baas et al., 2011; Baker and Baas, 2020).

The same very common convolute laminae can be related to an interplay between fine-grained sediment (silt and mud) and cyclic-wave loading associated with multidirectional combined flows (see Tinterri et al., 2016). This process must have been particularly efficient during the deposition of Unit C that can be characterized by an alternation of convolute lamine and low-amplitude bedforms that can pass laterally into slurry facies with pseudonodules (**Figure 8**). This transition can be related to the increase in cyclic-wave loading and mud percentage in decelerating combined flows able to form transient flows characterized by progressive attenuation of the near bed turbulence. Indeed, facies C record the vertical passage into the very thick mudstone unit D, whose thickness is due to the ponded condition. This last phase probably records a depositional phase similar to the cloud deflation phase by Patacci et al. (2015), which produces the final settling of fines from an essentially static cloud. Nevertheless, the presence of faint bandings within the upper mudstone unit does not rule out the occurrence of waning sloshing bores. Indeed, the concentration of cohesive mud in a flow can considerably affect processes of sediment deposition and resulting types of deposit (Amy and Talling, 2006; Talling et al., 2012). Investigating bedload transport and deposition of clay floccules, Schieber and Southard (2009) clearly showed that this process can occur at flow velocities that transport and deposit sand, pointing out that the formation of floccule ripples develop into low-angle foresets and mud beds appearing laminated after post-depositional compaction. Talling et al. (2012) showed that laminated mud (TE-1) and graded mud (TE-2) very likely result from floc settling at lower mud concentrations, while Ungraded (TE-3) mud intervals very likely form through *en-masse* consolidation of relatively dense cohesive mud suspensions due to gelling (see also McCave and Jones, 1988). From this point of view, it is plausible to think that a continuum from facies C to an uppermost massive ungraded mud of facies D can exist, related to the interaction between a progressive decrease in sloshing surges and dynamics of cohesive mud in the residual turbulent flow.

In conclusion, MCF megabeds fit very well with the model by Patacci et al. (2015) with a northeastward primary flow overlaid directly by a south-westward reversing flow separated by a density interface that can produce the RLs (see **Figure 8**).

4 SOLIGNANO FLYSCH AND MARNOSO-ARENACEA FORMATION CONFINED AND PARTIALLY CONTAINED BEDS

4.1 Introduction

The Solignano flysch (late Campanian-Maastrichtian in age) is part of the helminthoid flysch of the northern Apennines, such as the MCF (see location map in **Figure 7A**). Like the latter, the Solignano flysch is characterized by three main types of beds, namely: 1) micritic-marly beds, 2) arenitic-siliciclastic beds and 3) mixed beds exhibiting a basal arenitic-siliciclastic unit grading upward into a micritic-marly interval (Fontana et al., 1994). Some of the mixed beds can be megaturbidites showing characteristics similar to that of the MCF megabeds except for the fact that the Solignano beds are more siliciclastic and coarser than those of the MCF and are often characterized by erosive massive sandstone units rich in mudstone clasts.

The Solignano megabeds are always characterized by flute casts indicating a primary flow directed towards the northwest and ripples, vergent convolute laminae and flame structures, located just above the base, indicating paleocurrents exactly in

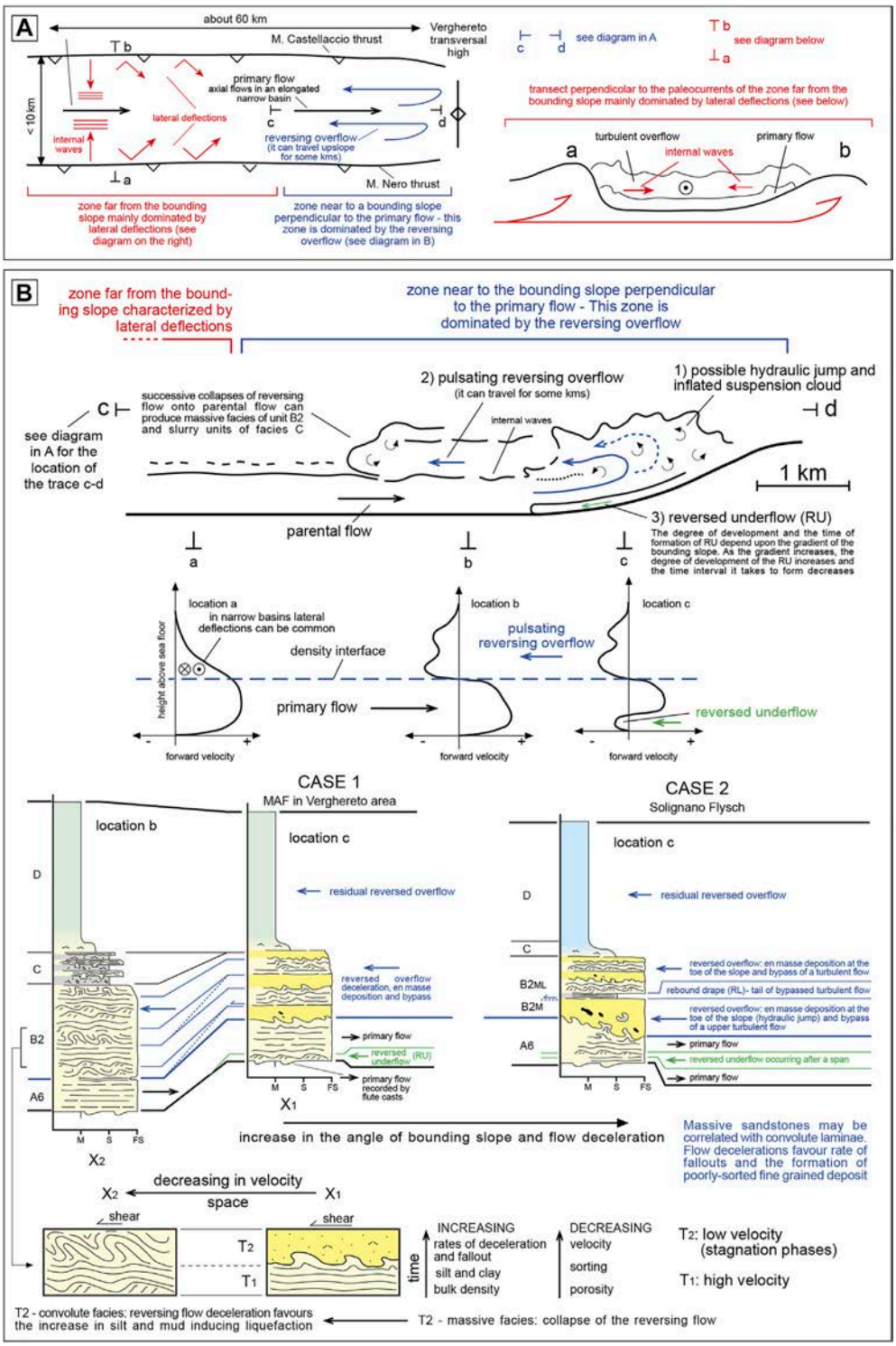

FIGURE 10 | (A) Schematic paleogeography of the MAF inner basin in which the main reflection processes related to the lateral and frontal basin margins are illustrated. Trace a-b indicates a cross-section perpendicular to the paleocurrents and to the main structural alignments represented by the M. Nero and M. Castellaccio thrusts (i.e., the lateral margins of the basin). Conversely, trace c-d indicates a cross-section parallel to the main structural alignments but perpendicular to the Verghereto high in a distal basin plain (see **Figures 2B,C**; modified from Tinterri and Muzzi Magalhaes, 2011). **(B)** Depositional model describing a flow perpendicularly impinging the Verghereto structural high (inspired by Howlett et al., 2019; see also Patacci et al., 2015). The model tries to link the facies variations in a direction towards the bounding slope with the different flow phases occurring during the reflection process. Below, a scheme illustrating facies and processes at the basis of the relationship between massive facies with load casts (near the bounding slope) and convolute laminae (in more distant zone).

the opposite direction, i.e., towards the southeast. This evidence allows an interesting comparison with the contained and reflected beds of the MAF near the Verghereto transversal tectonic feature, described by Tinterri et al. (2016) (see their **Figures 5**, **6**).

4.2 Description

The most part of the Solignano beds and megabeds are composed of a basal laminaset made of plane-parallel laminae (Facies A6) passing upward (sometimes through a first fine-grained drape, RL) into an alternation of ripples and vergent convolute laminae generally indicating paleocurrents directed towards the southeast (i.e., in the opposite direction vs. those indicated by the flute casts), (see Facies B2 in **Figure 9**). This laminated facies is often overlain by a massive fine-grained sandstone (Ta Bouma division) where mudstone and laminated sandstone intraclasts, eroded from the underlying unit, can be common. The base of the massive unit is erosive and is usually characterized by load and flame structures indicating paleocurrents towards the southeast and for this reason this facies is indicated as B2M (see **Figures 9A,B**, **Supplementary Figure S2A** and **Supplementary Table S1**). The grain-size analysis in thin section shows that these basal facies have the same grain-sizes, i.e., fine-grained sandstones (**Figure 9A**).

In general, above the first basal massive facies, there is a fine-grained drape rich in carbonaceous matter, mica and foraminifera (2nd RL in **Supplementary Figure S2D**), which divides the basal units from upper laminasets dominated by an alternation of ripples and vergent convolute laminae showing paleocurrents in the opposite direction (i.e., towards the south-southwest, see facies B2 in **Figure 9** and **Supplementary Figures S2B,C**). Sometimes, laminasets of this type are alternated with massive units with ball and pillows whose thickness tends to decrease upward; this facies has been indicated as B2ML (see **Figures 9C,D**, **Supplementary Figures S2E, S3** and **Supplementary Table S1**). These types of B2 facies passes upward into a very thick marlstone unit (facies D) through facies C made of silty very fine-grained sandstone dominated by soft-sediment deformations in which pseudonodules and contorted very thin laminasets characterized by ball-and-pillows, can still be recognized (**Supplementary Figure S2F**).

The Solignano bed types show strong analogies with the contained-reflected beds of the MAF near the Verghereto structural high, which is oriented perpendicularly to the general paleocurrents directed towards the SE (Unit IV by Muzzi Magalhaes and Tinterri, 2010, **Figure 10B**). These beds, 4 km away from the structural high, are composed of fine-grained sandstones characterized by even and parallel laminae passing upward into an alternation of vergent convolutes and ripples indicating reversing palaeocurrents directed towards the W and WNW (i.e., in the opposite direction vs. those indicated by sole casts directed towards the Verghereto high, see **Figures 1C**, **10B**). However, many contained-reflected beds in this zone are characterized by reversing ripples even in the most basal part of the beds, whereas the vertical passage into thick mudstone unit D is recorded, again, by a type-C unit characterized by an alternation of slurried units made of very fine sandy siltstone and thin laminasets composed of small-scale anisotropic hummocky-type structures characterized by ball and pillows and pseudonodules. These bed types pass downcurrent (i.e., towards the structural high) into beds composed of plane or slightly undulated laminae passing upward into an alternation of vergent convolute laminae, reversing ripples and massive units characterized by load structures, very similar to those described in the Solignano Flysch (see **Figure 10B**). In these zones, near the structural high, the vertical passage into the mudstone unit D tends to occur without the development of any unit C (**Figure 10B**). Essentially, the general model of **Figure 10B** emphasizes the facies tract of the beds characterizing the MAF in the Verghereto area and Solignano Flysch.

4.3 Interpretation

Facies B, C and D of the Solignano Flysch and the MAF beds in the Verghereto area are consistent with the facies categories introduced by Tinterri et al. (2016). In particular, these beds show many analogies with bed types cropping out in the Sorbas basin (southern Spain) and described by Haughton (1994), Haughton (2001).

In the MAF, for example, the beds towards the Verghereto structural high are all dominated by sedimentary structures indicating a very important role of the reversing flow and are generally characterized by a progressive increase, towards the bounding slope, in thin massive units with basal load casts (see **Figure 10**). This evidence can be interpreted as linked to an increase in deceleration and fallout rates and, more probably, to the collapse of the reversing-reflected flow that must occur in a pulsating way as testified by the alternation of laminated and massive units characterized by load casts near the bounding slope (see Postma et al., 2009; Tinterri et al., 2016).

More precisely, following the experimental phases described by Patacci et al. (2015) and Howlett et al. (2019), the basal facies, consisting of even or slightly undulated parallel basal laminae with flute casts indicating paleocurrents towards the NE, can be interpreted as recording the basal underflow directed against the bounding slope (Facies A6). However, the occasional occurrence of reversing ripples exactly at the base of the beds may suggest basal reversing flows consistent with the basal flow reversal by Patacci et al. (2015) or with the back squeezed underflow by Howlett et al. (2019) (see **Figures 1A,B**). Indeed, in this case, the structural high is relatively near (few kms) and flows impinge perpendicularly the bounding slope as in the aforementioned laboratory experiments.

Conversely, the facies characterized by the alternation of reversing ripples and vergent convolute laminae (Facies B2) can record the reversed overflow. As mentioned above, this alternation tends to evolve, moving towards the bounding slope, into a facies constituted by an alternation of even and parallel laminae and massive units with load casts (Facies B2M and B2ML, see **Figure 10B**). This lateral facies change can be related to a pulsating reversed overflow characterized by stagnation phases due to the repeated collapse, against the bounding slope, of the reflected overflow (Patacci et al., 2015; see also; Howlett et al., 2019). These stagnation phases must have produced a high rate of fallout near the obstacle generating massive units with load casts and relatively lower fallout rate far

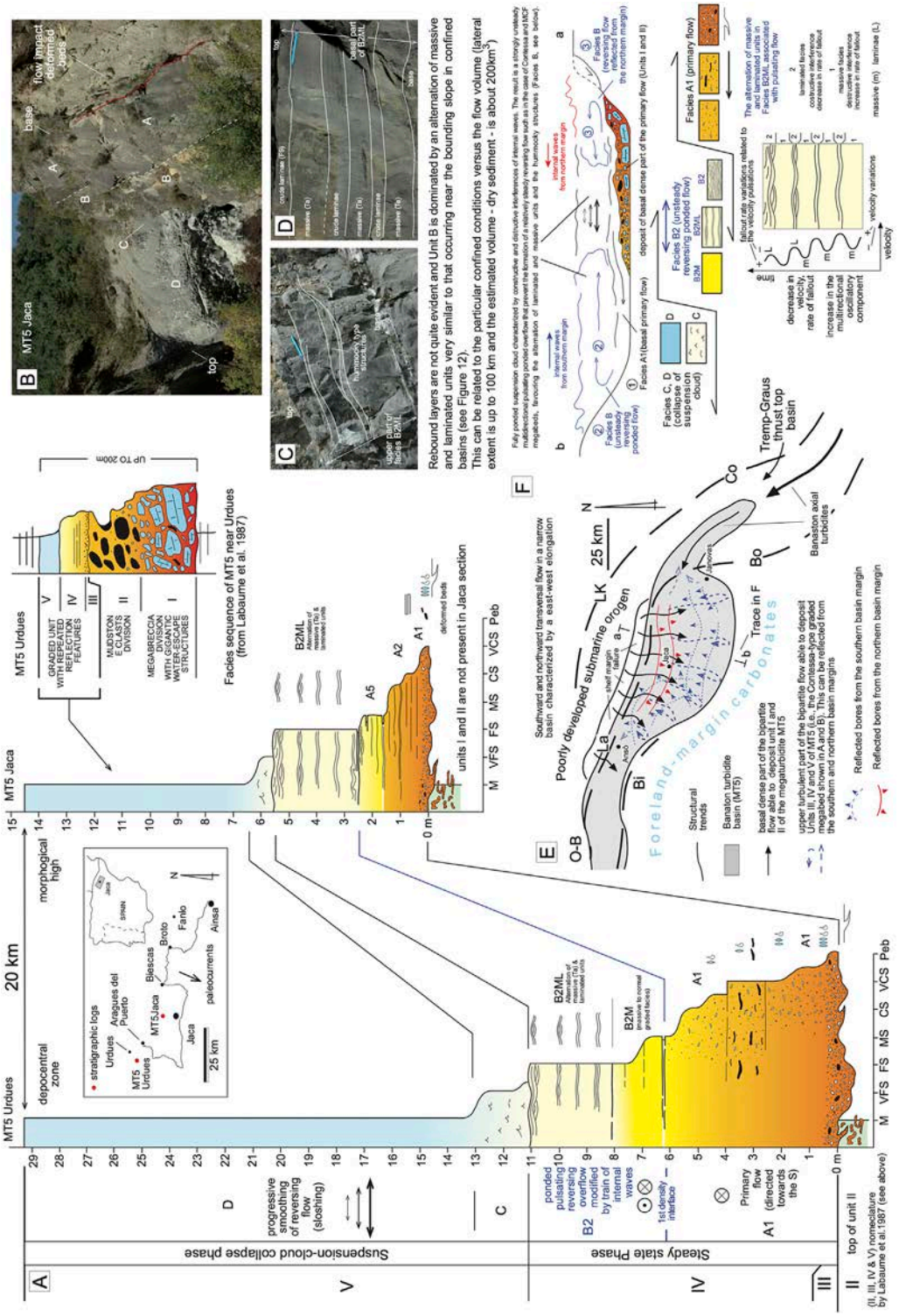

FIGURE 11 | (A) Description and interpretation (on the basis of the flow phases introduced for the CKB) of the megabed characterizing the upper part of megaturbidite MT5 in the Banaston basin (south western Pyrenees). In the upper part of A, the complete facies sequence of the MT5 with the five divisions introduced by Labaume et al. (1983), Labaume et al. (1987) can be observed; **(B)** The MT5 cropping out to the north of Jaca (see A for the related stratigraphic Log); **(C)** Hummocky-type structures characterizing the upper part of facies B2 in the stratigraphic Log near Urdues (see A); **(D)** Detail of facies B2ML in the stratigraphic log to the north of Jaca (see A); **(E)** Diagram showing the relationship between basin morphology and the flow able to deposit the MT5. This model hypothesizes a source area located in the northern margin as indicated by Labaume et al. (1987). The basin geometry and the main tectonic structures are from Remacha et al. (2005). **(F)** Depositional model and facies tract of the upper megabed of the MT5, below a diagram illustrating the formative processes of facies B2ML.

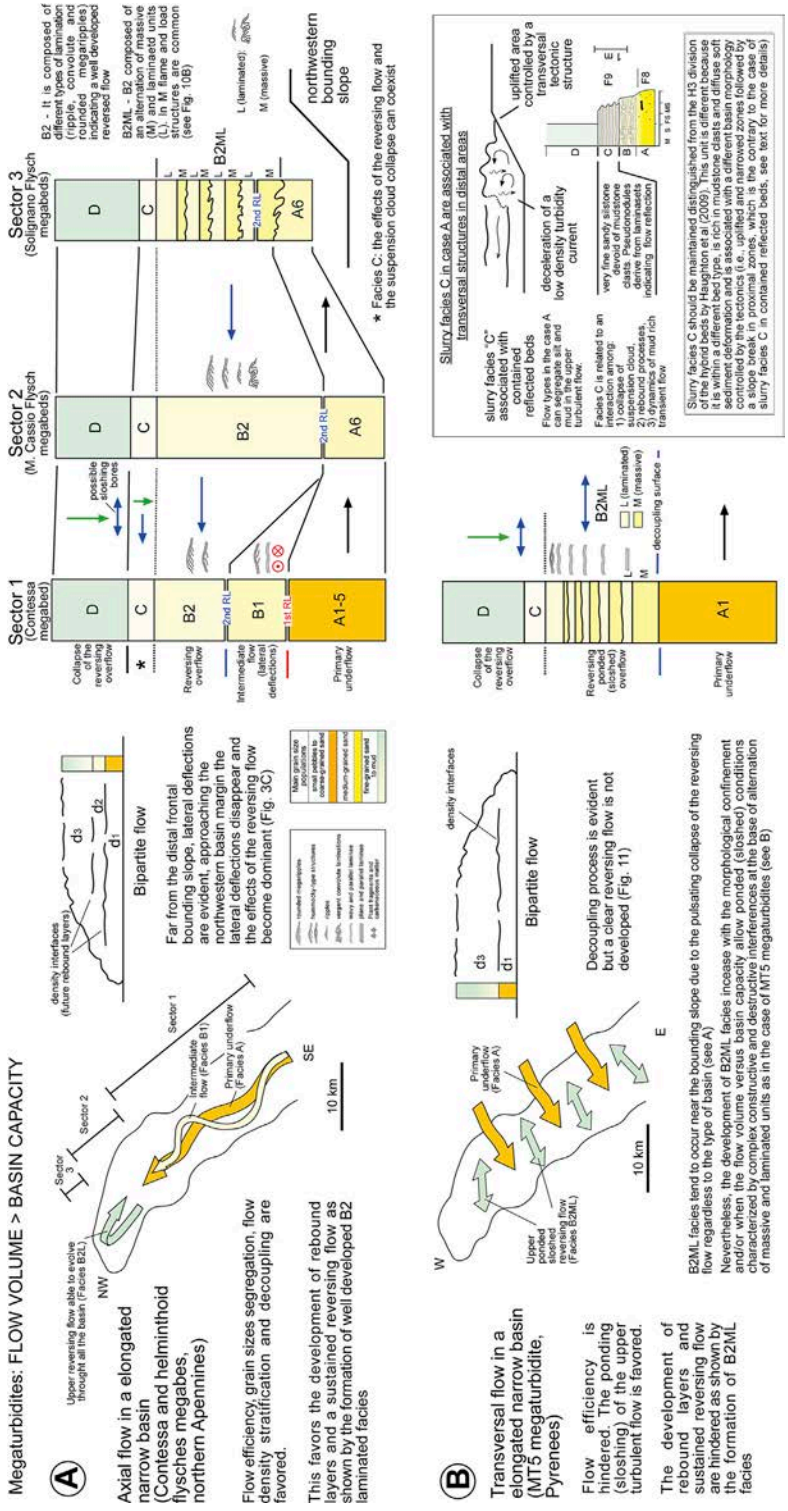

FIGURE 12 | Depositional models that summarize the different study cases in this work. In **(A)**, the cases of the Contessa Key bed and helminthoid flysches, which are deposited by axial flows in elongated and narrow basins. In **(B)**, conversely, the case of megaturbidite MT5 in the south western Pyrenees deposited by a flow transversal to an elongated and narrow basin.

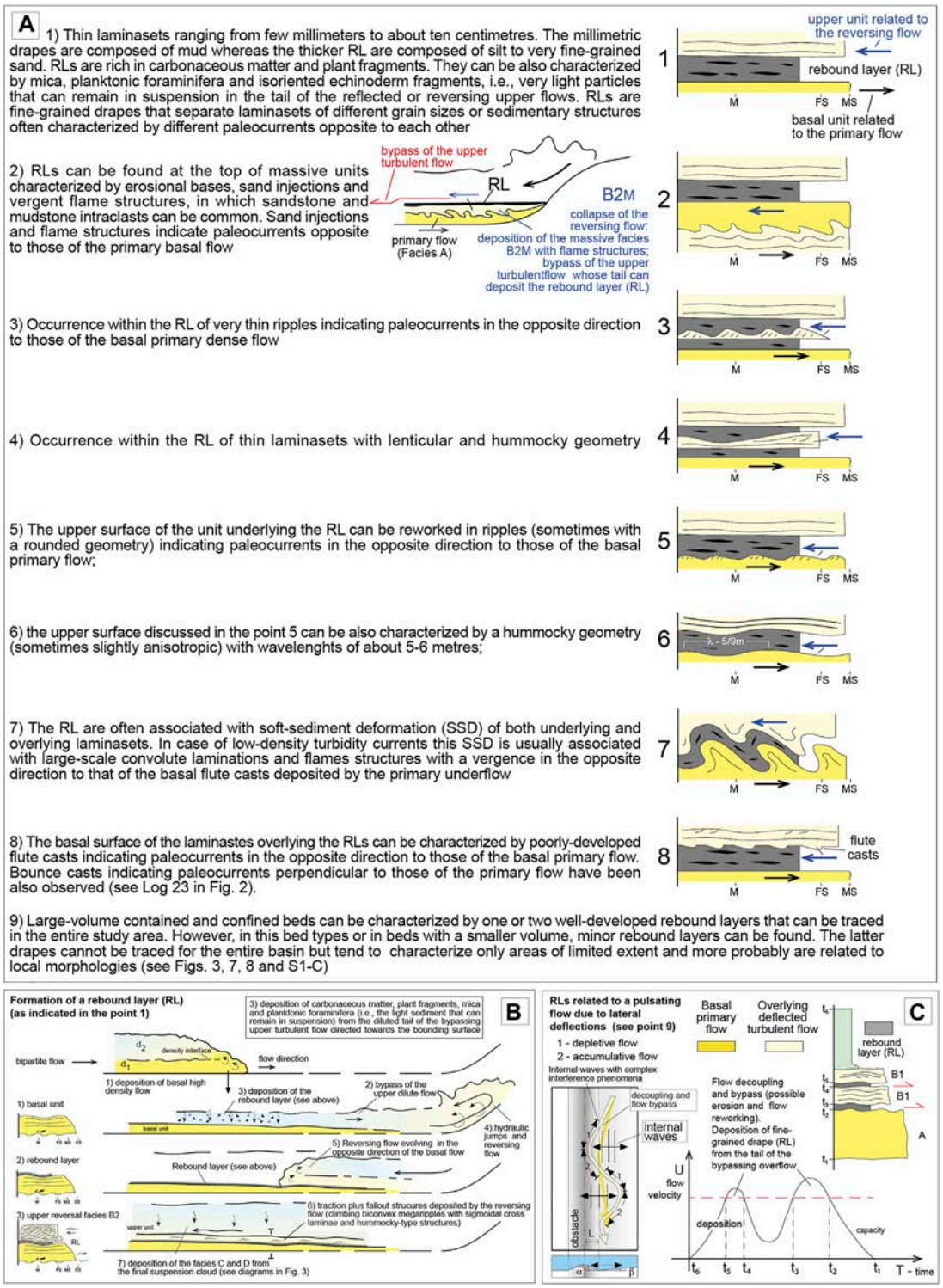

FIGURE 13 | (A) Main sedimentary characteristics of the different types of rebound layers (RLs). In the point 2 a scheme illustrating the formation of a RL associated with the collapse of a reversing flow induced by a bounding slope can be also observed; **(B,C)** Two different depositional models showing how RLs can form, are shown (see points 1 and 9). Diagram in C is inspired from Kane et al. (2009) and Tinterri et al. (2016).

from the bounding slope generating convolute laminae. In other words, in zones far from the bounding slope the fallout rates associated to the stagnation phases may be sufficient to produce deposits rich in silt and mud that can favor liquefaction processes and consequently convolute laminae (see also Tinterri et al., 2016; Gladstone et al., 2018). From this point

of view, a possible relationship is proposed between massive units and convoluted laminasets as indicated in **Figure 10B**.

In these situations, however, constructive and destructive interferences between different trains of reflected bores or internal waves may further contribute to the pulsating nature of the reversed overflow and to the convolute formation through cyclic-pressure variations (Tinterri et al., 2016).

This facies B2, in turn, can pass upward into a facies C characterized by a fine-grained sandy siltstone that can be interpreted as a slurry facies (sensu Lowe and Guy, 2000). This facies is generally characterized by an alternation of thin slurry units and laminasets consisting of large-scale hummocky-type structures and low-angle megaripples that can indicate paleocurrents opposed to those of flute casts. It tends to taper and disappear towards the structural high, presumably above the bounding slope (**Figure 10B**). This facies is interpreted as the collapse of the fine-grained sediment (very fine-grained sand, silt and mud) characterizing the residual reversed flow at the toe of the obstacle where the slope change and the deceleration degree are the highest. In this process, however, a key role must have been played not only by the dynamics of the fine-grained sediment (e.g., Schreiber et al., 2007; Baas et al., 2011) but also by reflection processes as testified by the occurrence of laminated units characterized by reversed sedimentary structures. Consequently, the origin of this facies cannot be merely a simple collapse of the reversing flow as indicated by Patacci et al. (2015) but rather, as the alternated facies suggest, in the same way of facies B2, a pulsating collapse of the mud-rich residual reversing flow with the deposition of slurry facies, during the deceleration phases in which the cohesive strength of mud prevails, and laminated units during acceleration phases in which traction-plus-fallout processes must prevail. In the latter case, combined flows (see Tinterri et al., 2016) and the dynamics of the fine-grained sediment (mud and silt) (see Baker and Baas, 2020) may both contribute to produce the hummocky-type structures and large-scale low-angle megaripples. The erosion of mud on the bounding slope by the reflected flows as indicated by Bell et al. (2018) may surely contribute to the formation of slurry facies, even if, in the case of MAF, this facies is not characterized by the presence of mudstone clasts but only by load structures, such as pseudonodules, deriving from laminated units. Facies C, therefore, is interpreted as mainly associated with the pulsating collapse of the mud rich residual reversing flow at the toe of the structural high where the slope change produces the highest rates of deceleration (see Sumner et al., 2009; Baas et al., 2011). Following the experimental phases described by Patacci et al. (2015) facies C and the thick mudstone facies D can record the final phase of suspension-flow collapse modified, however, by the aforementioned processes.

The Solignano Flysch beds (**Figure 9**) are very similar to those described in the Verghereto area and thus are interpreted as recording similar sedimentary processes and similar basin morphologies, i.e., primary flows directed towards a northwestern obstacle and reflected flows in the opposite direction, i.e., towards the southeast. This evidence, together with the occurrence of well-developed rebound layers above thick massive units characterized by folded mudstone and sandstone clasts and erosional bases with flame structures indicating reversed paleocurrents, are evidence of a more drastic deceleration and collapse of the reversing flow (**Figures 9**, **10B**). This is probably due to the obstacle being in closer proximity or a more pronounced slope change than those of the MAF beds in the Verghereto area. In this case, it is plausible to think that decoupling processes, with a drastic collapse of the basal part of the reversing flow and bypass of its uppermost turbulent portion, can occur in a very efficient way with the consequent formation of a tail able to deposit a fine-grained drape rich in plant fragments, carbonaceous matter, mica and planktonic foraminifera, i.e., particles able to remain more efficiently in suspension (**Figure 9A**). Above this first rebound layer, in the same way as for the MAF beds, facies B2ML is characterized by an alternation of vergent convolute laminae, reversing ripples and massive units with load casts, which can be interpreted as associated with a pulsating reversing flow suffering repeated gravitational collapses and re-accelerations. In the same way, the slurry Facies C, with soft-sediment deformation, and Facies D can record the final phase of suspension-flow collapse where, however, the faint laminations of facies D suggest traction-plus-fallout processes in mud sediment as indicated by Schieber and Southard (2009).

Essentially, contained-reflected beds characterized by thin massive units with load structures can be present not only in small-scale confined basin, as indicated by Patacci et al. (2015), but also in relatively large basins as in the case of the MAF beds deposited in a foredeep and M. Cassio and Solignano helminthoid flysches deposited in an ocean basin. Consequently, their presence should be ascribed to the proximity of a bounding slope rather than to the dimension and the degree of basin confinement, even if the data coming from the MAF and MT5 megaturbidite in the Pyrenees show that these massive units within the strata become more and more evident as the degree of tectonic confinement versus flow volume increases (see below). In the same way, the rebound layers (RL) near the bounding slope seem to be more developed in large-volume beds in which the decoupling processes are enhanced by flow stratification and by the degree of flow deceleration related to the proximity of the obstacle and the size of the slope change.

5 MT5 MEGATURBIDITE (SOUTH WESTERN PYRENEES)

The considerations just made seem to be confirmed by the facies analysis of the calcarenite at the top of the MT5 megaturbidite in the Banaston turbidite system (south-western Pyrenees) (**Figure 11**). This megabed, deposited at the top of very thick calcareous megabreccia, is related to the upper high-density

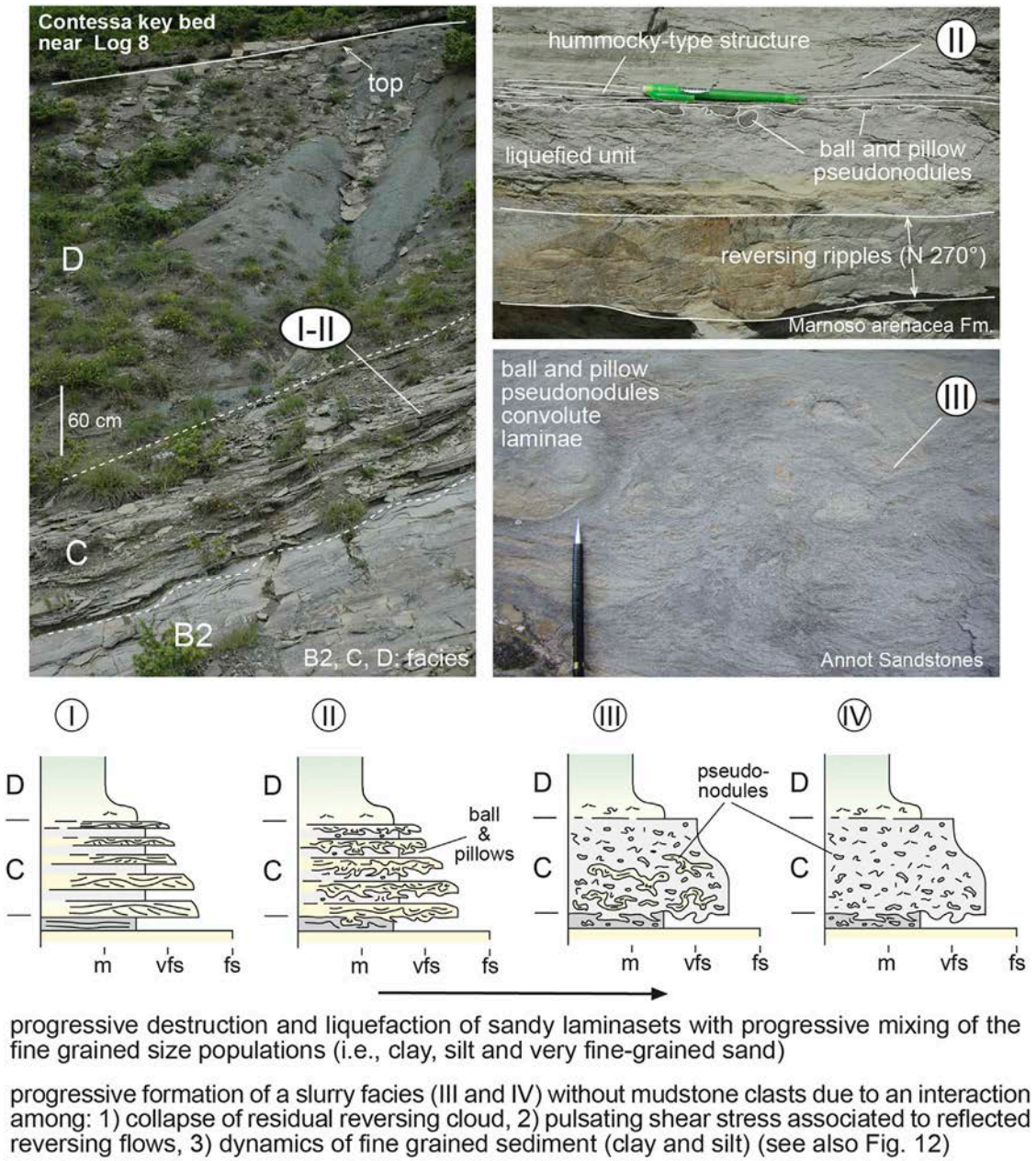

FIGURE 14 | Diagrams illustrating the different types of slurry facies C in relation to the progressive increase (from I to IV) in soft sediment deformation with the consequent destruction of the sandy laminasets.

turbidity current characterizing the bipartite flow able to deposit the MT5 (Labaume et al., 1987; Mutti et al., 1999; Ogata et al., 2012; see also **Figure 11**). Consequently, this megabed shows strong analogies with the megabeds discussed so far and especially with those in **section 4** (see **Figure 9**); indeed, it consists of a basal coarse-grained massive facies A1 passing upward into a facies B2ML made of an alternation of fine-grained laminated (L) and massive (M) units where the former are mainly characterized by hummocky-type structures and low-angle wavy laminae (**Figures 11A,C,D**). The rebound layers are not well developed and are often absent (**Figure 11A**).

The main difference from the Contessa and helminthoid flysch megabeds is that the MT5 is deposited by a flow transversal to the elongated and narrow basin of the Banaston turbidite system (**Figures 11E,F**). Therefore, these conditions can create a fully ponded suspension cloud (*sensu* Patacci et al., 2015) where the upper reversing flow, which can be reflected from both the southern and northern margin, can combine itself with various types of bores coming from

different zones due to the basin geometry (**Figure 11E**). Consequently, the formation of complex constructive and destructive interference processes must result in a strongly unsteady multidirectional pulsating ponded overflow. Said overflow prevents the formation of a relatively steady reversing flow and, consequently, of well-developed reversing megaripples and rebound layers, such as in the case of the Contessa and MCF megabeds, and favours the formation of the alternation of laminated and massive units (Facies B2ML) and the hummocky-type structures (**Figure 11F**). Facies B2ML is related to a pulsating flow where the massive units can be associated with destructive interferences, which cause velocity to decrease and the fallout rate to increase, while the laminated units can be related to constructive interferences with consequent increase in velocity and decrease in the fallout rate (**Figure 11F**). The same hummocky structures, low-angle wavy and plane and parallel laminae are favoured by the unsteady multidirectional nature of the overflow as indicated by Tinterri (2011).

6 DISCUSSION: DEPOSITIONAL MODEL FOR FULLY-PONDED CONFINED BEDS

The depositional model and facies tracts proposed for the megaturbidites of the MAF (Contessa bed) and helminthoid flysches (**Figures 3**, **8**) are essentially consistent with depositional phases 3 and 4 of the recent laboratory experiments by Patacci et al. (2015) (see also Howlett et al., 2019, **Figure 1**). In these geological settings, axial turbidity currents evolving towards NW in narrow NW-SE stretched basins, can maintain the flow efficiency and have the time for producing a well-developed reversing flow (see **Figure 12A**). The field data, indeed, indicate that these megaturbidites are characterized by four parts recording the basal primary flow (facies A), an intermediate flow characterized especially by lateral deflections and a reversing flow (facies B1), a well-developed reversed flow (facies B2) and an upper residual flow recording the final collapse of the suspended load (facies C and D) (**Figures 3**, **8**, **12A**). More precisely, facies A is consistent with the underflow (*sensu* Patacci et al., 2015) directed towards the bounding slope where the downcurrent facies change from facies A1 to facies A6 describes the evolution from a high-density to a low-density turbidity current (**Figure 3**). Conversely, facies B is well consistent with the development of an upper reversing flow, even if the field data deriving especially from the CKB highlight that, between basal facies A and facies B2 characterized by megaripples indicating a south-eastward reversed flow, there is an intermediate facies B1 in which the sedimentary structures indicate a flow characterized by SW-NE oriented lateral deflections. It is interesting to note that facies A, B1 and B2 are well separated by two evident rebound layers (1st and 2nd RL in **Figure 12A**) that can be consistent with the internal density surfaces by Patacci et al. (2015). Finally, facies C and D can be related with the final phase of collapse of the residual suspended load cloud modified by a complex interaction between combined flows associated with rebound processes and the dynamics of a mud rich suspension which must control the formation of the slurry facies and low-angle hummocky-type structures and megaripples.

However, the evidence that facies B1 is not present in the MCF megaturbidites more probably depends upon their proximity to the northern basin margin where the effects of the reversed flows can be much higher than those of lateral deflections that, conversely, should be more evident away from the northern basin margin as it occurs for the CKB and MAF beds (see **Figure 10A** and sector 2 of **Figure 12A**; see also Tinterri et al., 2016).

This evidence is also confirmed by the data of the MAF beds in the Verghereto area and of the Solignano flysch beds (**Figure 10**). Indeed, these strata are located very near to a morphologic obstacle and can give important information about the reflection phases near the bounding slope (i.e., phase 1 by Patacci et al., 2015; see also Howlett et al., 2019). These beds are all dominated by sedimentary structures indicating a well-developed upper reversing flow (**Figure 10**), also testified by progressive increase, towards the bounding slope, in thin massive units with load casts alternated with laminated units characterized by ripples, convolute laminae and hummocky-type structures indicating reversing paleocurrents (facies B2ML in **Figure 12A**). This facies can be related to the pulsating collapse of the reversing overflow consistent with repeated stagnation phases as described in the laboratory experiments (Patacci et al., 2015; Howlett et al., 2019). These stagnation phases can be also at the basis of the formation of slurry facies characterizing facies C (**Figure 12A**).

Facies B2ML featuring this type of alternation is also common in the upper megabed characterizing the MT5 in the southern Pyrenees (**Figure 12B**). This megabed is deposited by a flow transversal to an elongated narrow basin, and its large volume versus basin capacity tends to hinder the generation of a sustained reversing flow and rebound layers favoring the formation of a fully-ponded sloshing pulsating overflow able to deposit alternations of laminated and massive units that must be related to constructive and destructive interference processes (**Figure 12B**).

The comparison between field and experimental data allows more detailed discussions of some key topics characterizing contained-reflected beds, such as the significance of rebound layers (RL), the slurry deposits of facies C and the low-angle sedimentary structures featuring facies C and B.

6.1 Sedimentary Characteristics and Formation of the Rebound Layers

Although discussed briefly by Pickering and Hiscott (1985) and Edwards et al. (1994), rebound layers (RLs) are one of the most common and diagnostic structure of fully-ponded contained and confined beds (see Tinterri and Muzzi Magalhaes, 2011; Tinterri et al., 2016). The comparison between MAF megaturbidites and helminthoid flysches shows the main sedimentary characteristics of these rebound layers that are summarized in **Figure 13**.

On the basis of these sedimentary characteristics, RLs are interpreted as recording the deposition of a residual very fine-grained suspended load during a relatively quiescent period after

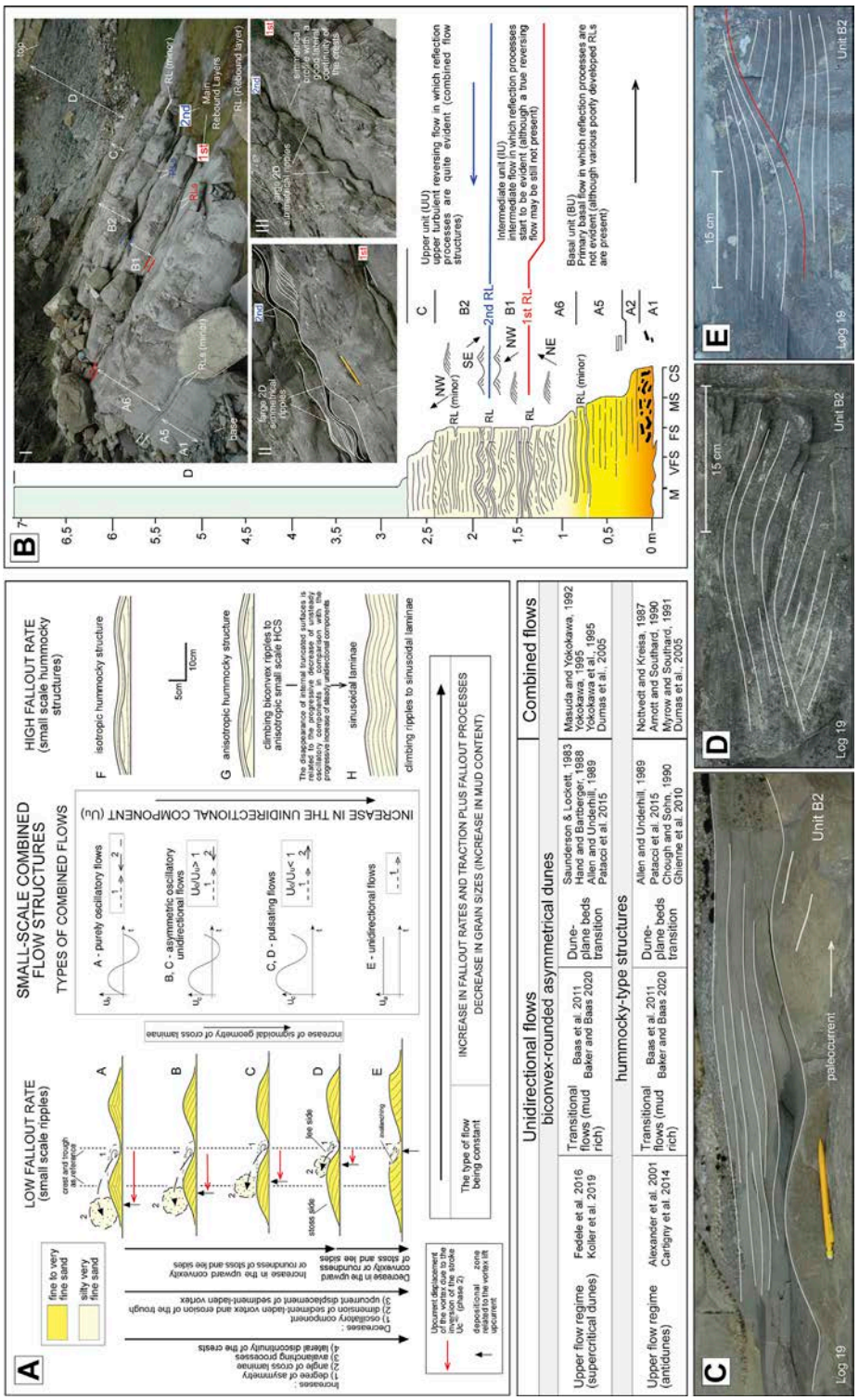

FIGURE 15 | (A) Facies scheme summarizing the transformations of the ripples and megaripples related to different types of combined flows on the basis of field observations and flume experiments available in the literature. Two cases related to two different fallout rates and to decreasing grain sizes are also shown (from Tinterri, 2011). Below, a table illustrating the main type of processes able to form biconvex megaripples; some main references are also shown (modified from Tinterri, 2011); **(B)** A Contessa-type megabed coming from the Tufiti di Tusa Formation in southern Italy. Worth noting are the magnificent examples of symmetrical megaripples with sigmoidal cross lamination very similar to case B shown in A; **(C–E)** example of biconvex megaripples with sigmoidal-cross laminae and hummocky-type structures coming from the CKB in Log 19 (see **Figures 3**, **4** for the location of the Log).

the deposition of the basal sandstone by the primary flow (**Figure 13B**). Indeed, during this period, the tail of the upper bypassed flow can deposit a thin drape of mud or very fine-grained sand characterized by particles able to remain easily in suspension, as indicated in point 1. The reversed flow generally is not able to erode the fine-grained drape of the RL; in fact, flute casts indicating reversed paleocurrents at the base of the laminaset just above the RL have been observed in only one case (see point 8, **Figure 13A**). However, the sedimentary characteristics listed in points 2, 3, 6 and 7 (**Figure 13**) show that RLs could also be associated with the tail of the reversed flow; ripples at the top of the basal sandstone unit clearly show that the flow had already been reflected before the RL deposition. Likewise, RLs just above massive units with flame structures indicating reversed paleocurrent can be evidence of an efficient decoupling process with the collapse of a basal part of the reversing flow and the bypass of an upper more diluted turbulent flow whose tail can deposits the RL drape (**Figure 13A**, point 2). In general, this case is more likely to occur in zones near the obstacle and, indeed, the collapse of a part of the reversed flow can be related to a slope change with the possibility to form an internal hydraulic jump, ball and pillows and flame structures due to the high rate of fallout (see Postma et al., 2009; Tinterri et al., 2016). Folded RLs due to soft-sediment deformation, which is usually represented by large-scale vergent convolute lamination (point 7, **Figure 13A**), can be related to a similar process or a pulsating shear stress associated with a combined reversed flow (see Tinterri et al., 2016). The same thin laminasets within the RL, characterized by reversing ripples (see point 3), are evidence that, at least in part, the fine-grained drape is deposited by the reversing flow even if these ripples can be also deposited by local reflection processes associated to local morphologies. Indeed, their geometry is usually characterized by strong lenticularity, such as the laminasets composed of hummocky-type structures (point 4), that, besides indicating a combined reversed flow, can be evidence of compensation phenomena of the hummocky geometry of the basal sandstone upper surface (see point 6 in **Figure 13A**). This geometry can be related to reworking processes associated with the bypass of upper low-density primary flow as well as reversing flow that, also given the presence of biconvex ripples, could have combined flow characteristics.

The possibility that RLs can be associated with local flow reflections is also substantiated by the presence of minor RLs traceable only over short distances. In this case, RLs may be related to unsteady pulsating flows reflecting local seafloor reliefs and recombination of deflected reversed flows with a mechanism similar to that described by Kane et al. (2009) as shown in **Figure 13C** (see also Patel et al., 2021).

However, it appears evident that well-developed RLs that can be traced throughout the basin are those associated with megaturbidites deposited by large-volume turbidity currents capable of crossing the basin several times (point 9 in **Figure 13A**). In particular, the comparison between CKB and MT5 megabeds (**Figure 12**) suggests that the development of RLs is associated with highly-stratified axial flows in elongated and narrow basins, as in the CKB where the maintenance of flow efficiency allows the formation of a well-developed reversing flow. In this case, RLs can be consistent with the internal density surfaces along which decoupling processes can occur and internal waves at different frequencies can propagate (see Tinterri, 2011; Patacci et al., 2015). This process can be at the basis of the combined flow structures as well as the hummocky surface, which features the top of the basal sandy unit A6 deposited by the primary flow.

6.2 Formation and Significance of Slurry Facies in Contained and Confined Beds

The formation of slurry facies within contained-reflected beds in distal basin plains is another important topic that deserves to be discussed. These facies indicated in this work as facies C, record the passage between the fine-grained sandstone facies B and the uppermost mudstone facies D. In general, the slurry unit is composed of a very fine-grained sandy siltstone and is characterized by a continuum of facies whose end members are: 1) a completely homogeneous facies rich in soft-sediment deformations, such as contorted pseudonodules and convoluted laminae and 2) an alternation of thin slurry units and laminasets characterized by hummocky-type structures and low-angle megaripples indicating paleocurrents opposite to those of the flute casts and, in some cases, opposite one to the other (**Figure 14**). The latter facies passes to the completely homogenized facies through a progressive increase in the soft-sediment deformation represented by load structures (ball and pillows and detached pseudonodules) as shown in **Figure 14**. It is considered important to stress that mudstone intraclasts were never found in any facies C of the cases studied.

This facies is a typical characteristic of contained-reflected beds and was discussed for the first time by Pickering and Hiscott (1985) and later by Haughton (1994), Remacha et al. (2005), Muzzi Magalhaes and Tinterri (2010). More recently, this facies formation process was discussed also by Patacci et al. (2015) and Bell et al. (2018). The former gives more emphasis to the processes of cyclic-wave loading linked to various types of internal waves or bores resulting in the slurry facies, whereas the latter tends to give more emphasis to the collapse phases of fine residual flows. In particular, Bell et al. (2018) see the formation of this type of slurry as due to the collapse of a deflected turbidity current enriched of mud through erosion processes occurring on the bounding slope. In this study, however, the slurry facies is always devoid of mudstone clasts and, in many cases, also of arenaceous pseudonodules, showing a poorly-sorted liquefied homogeneous very fine-grained sandy siltstone.

From this point of view, it is more likely that this facies is the result of a combination of several factors rather than just one, such as: 1) the collapse, enhanced by the basin morphology, of the fine residual part of a contained-reflected current where the presence of bores still slowly move back and forth across the basin cannot be completely ruled out, 2) the dynamics of combined flows characterized by pulsations of different frequencies. Lower frequency pulsations linked to the alternation of the flow stagnation and re-acceleration phases can contribute to the formation of the alternation of slurry and laminated units, whereas high-frequency internal waves can contribute to the formation of combined flow structures

and to the liquefaction processes linked to cyclic shear stresses, 3) the dynamics of mud rich turbulent flows that, through the formation of transitional flows (sensu Baas et al., 2009, Baas et al., 2011), can favor the formation of slurry units and low-angle mixed sand-mud bedforms (see below).

Facies C tends to be associated with intrabasinal morphologies that favour flow decelerations and an increase in sediment fallout, as in the case of CKB where this facies is better developed near important transversal tectonically-controlled highs (see **Figures 2**, **3**). Likewise, in contained and confined turbidites having relatively small volumes (in comparison with megaturbidites), facies C tends to develop in distal basin plains against important morphological barriers, such as in the case of MAF beds at the toe of the Verghereto structural high (**Figure 10B**). This is evidence that the role of the collapse of fine-grained residual suspension is certainly fundamental, as well as reflection processes as testified by the occurrence of sedimentary structures indicating paleocurrents different one from the other and from those of the flute casts.

The progressive passage from a facies characterized by an alternation of different units to a well-developed homogeneous slurry facies must depend upon an increase in the fallout rate, related to the rate of deceleration and to an increase in silt and mud content towards the basal part of the flow, which favor the formation of transitional flow (see **Figure 14**).

Lastly, it is considered important to point out that this slurry facies C should be kept distinguished from the intermediate slurry unit of the classic tripartite hybrid beds as described by Haughton et al., 2009 (i.e., H3 division; see also Talling et al., 2004; Muzzi Magalhaes and Tinterri, 2010). The former, consisting of very fine-grained sandy siltstone rich in load structures without mudstone clasts, is associated with deceleration and reflection of low-density turbidity currents in basin plains against distal morphological obstacles. On the contrary, the latter consists of muddy sandstone rich in mudstone clasts and soft-sediment deformation produced by decelerations, induced by a gradient decrease, of mud-rich turbidity currents, whose mud enrichment must occur upcurrent, generally induced by a tectonic confinement that favor erosive processes (Tinterri et al., 2020; see **Figure 12**).

6.3 Asymmetrical Biconvex Megaripples and Hummocky-Type Structures

Contained-reflected beds usually show various typical bedforms that characterize especially facies B and C (**Figures 3**, **6**, **15**). These sedimentary structures are: 1) biconvex asymmetrical to symmetrical megaripples with sigmoidal-cross laminae, 2) isotropic to anisotropic small-scale hummocky-type structures, and 3) low-angle undulated laminae. Megaripples and hummocky-type structures are generally characterized by wavelengths of about 40–60 cm and are often associated with reversing flows since they indicate paleocurrents opposite to those of flute casts. Magnificent examples of symmetrical 2D megaripples separated by evident RLs can also be observed in another Contessa-type megabed in the Tufiti di Tusa Formation in the southern Apennines (see **Figure 15B**; see also Cerone et al., 2017). This evidence led to interpret these structures as related to combined flows deriving from the interference processes between reflected turbidity currents and different trains of internal waves or bores (Tinterri, 2011; Tinterri et al., 2016; see also Kneller et al., 1991; Edwards et al., 1994; Haughton, 1994). Indeed, experimental data show that an oscillatory component in combined flows, dominated by a unidirectional component, favours the formation of biconvex ripples and megaripples with sigmoidal-cross laminae (Yokokawa et al., 1995; Dumas et al., 2005). This is related to how the sand is redistributed by the vortices relating to forward and backward strokes of the oscillatory components (**Figure 15A**). In general, in a combined flow dominated by a unidirectional component, the sandy load lifted in suspension by the vortex formed in front of the lee side, associated with the stronger stroke, is not redistributed completely on the stoss side as in the purely oscillatory flows, but a large part of said load is deposited on the lee side near the brinkpoint, forming a bulge structure materialized by a convex lamina. The latter, joining with the lower part of the concave-upward foresets, produces a sigmoidal lamina. In these cases, however, an increase in the fallout rate or a decrease in grain sizes or a combination of both processes may favor ripple roundness and the vertical passage into small-scale hummocky-type structures (see Tinterri, 2011) (**Figure 15A**). In these cases, however, a contribution given by a supercritical unidirectional component producing asymmetrical rounded megaripples cannot be completely ruled out (see Fedele et al., 2016) (see table in **Figure 15A**).

It is also possible that the dynamics of mud and silt forming transient turbulent flows and mixed sand-mud bedforms can have played an important role (see Baker and Baas, 2020; Baas et al., 2021). This is particularly valid for the sedimentary structures characterizing facies C, which are made of muddy very fine-grained sandy siltstone.

Recent laboratory experiments, indeed, have shown that current ripples can transform into large-scale ripples and then into low-amplitude bedwaves, under decelerating sand-mud flows where the increase in viscosity due to mud-rich suspension can produce transitional flows with attenuated turbulence (Baker and Baas, 2020; Baas et al., 2021). The same vertical passage from megaripples into convolute laminae (see **Figure 10B**) can be associated with an increase in mud content as indicated by Tinterri et al. (2016) and Gladstone et al. (2018), which could be related to an increase in flow deceleration and fallout rate associated with stagnation or destructive interference phases of the reversed/deflected flow (**Figure 10B**). The same lateral facies variation in facies B, where alternations of megaripples and convolute laminae pass, towards the bounding slope, into alternations of even/undulated low-amplitude laminations and massive units with load structures, can be related to an increase in fallout and deceleration rate allowing a relationship between convolute laminae and massive units to be assumed, as indicated in **Figure 10B**.

7 CONCLUSION

This work discusses facies and processes of contained and confined beds of the MAF and helminthoid flysches in the northern

Apennines. In particular, thanks to the comparison of the Contessa megabed and some particularly significant megabeds of the MCF, on the hand, with the MT5 megaturbidite in the Pyrenees, a depositional model for fully-ponded beds, which is well consistent with the experimental data available in the literature (see **section 2**), can be proposed (see **Figure 12**). These megaturbidites, which are deposited by turbidity currents having larger volumes than those of the respective basins, are characterized by four main facies (A, B, C and D in **Figure 12**), whose characteristics change depending on whether the flows are characterized by an axial source (parallel to the basin axis), as in the case of the CKB and helminthoid flysches, or by a source transversal to the basin (perpendicular to the basin axis), as in the case of the MT5.

In the former case the lateral confinement favours the conservation of flow efficiency and the development of a steady phase 3 by Patacci et al. (2015) (**Figure 12A**). In this case, indeed, Facies A, consisting of six facies (A1 to A6), records the evolution of the basal primary underflow, while Facies B, made of two subfacies B1 and B2, records an intermediate flow with lateral deflections and a well-developed reversed overflow, respectively. Conversely, Facies C and D, consisting of a slurry facies C and a very thick mudstone unit D, record the final collapse of the suspended load characterizing a residual reversing flow (**Figures 3**, **8**, **12**). In the case of **Figure 12A**, facies A, B1 and B2, are usually separated by evident very thin fine-grained muddy drapes (rebound layer, RL) that can be related to the internal density surfaces highlighted also by flume experiments, along which decoupling processes separating the underflow from the reversing overflow can occur more easily (**Figure 13**). Facies C, however, tends to be more developed near the morphological highs, where the rates of deceleration, the dynamics of muddy transient flows and interference of reflected internal waves can play a key role in the formation of sandy siltstone slurry facies, when turbulent flows impinge perpendicularly a distal basin margin.

Conversely in the case of MT5 (**Figure 12B**), flows transversal to the basin axis tend to favor the formation of fully-ponded pulsating (sloshing) overflows hindering the generation of sustained reversing flows and, consequently, of evident rebound layers, favoring instead the deposition of alternations of laminated and massive units (B2ML facies) deriving from complex interference processes associated with pulsating overflows (**Figure 11**). A similar facies, however, can be also observed in the basins characterized by axial flows only near the basin margin where the pulsating collapse of the reversing flow dominates (see **Figures 10B**, **12A**).

This study shows that field studies integrating high-resolution physical stratigraphy, facies analysis and regional-structural geology are essential for a correct interpretation of any type of structure, at any scale, and, consequently, for tangible validation of experimental data from an applicative point of view.

DATA AVAILABILITY STATEMENT

The original contributions presented in the study are included in the article/**Supplementary Material**, further inquiries can be directed to the corresponding author.

AUTHOR CONTRIBUTIONS

RT contributed to the Conceptualization, Methodology, Investigation, Writing—original draft and Project administration; TM and PM contributed to the Investigation; All the Authors contributed to manuscript revision, read, and approved the submitted version.

ACKNOWLEDGMENTS

We would like to thank Alessio Tagliaferri, Alberto Piazza, Rogerio Soares Cunha, Vanni Pizzati, Elena Scacchia and Simone Lombardi for the discussions in the field and their help in the final editing phase. Luca Baruffini is thanked for the discussions on the helminthoid Flysches. Emiliano Mutti and Eduard Remacha are thanked for their teachings and discussions on the Hecho Group. We also wish to thank Dave Hodgson (Chief Editor), Rosanna Maniscalco (Guest Editor) and the reviewers Salvatore Milli and Giacomo Dalla Valle for their helpful and constructive comments which helped to improve the manuscript. This research was partially funded by ENI SpA and Petróleo Brasileiro S.A. (Petrobras). In particular, we thank Giancarlo Davoli (Eni) and Mario Carminatti (Petrobras).

SUPPLEMENTARY MATERIAL

The Supplementary Material for this article can be found online at: https://www.frontiersin.org/articles/10.3389/feart.2022.817012/full#supplementary-material

REFERENCES

Alexander, J., and Morris, S. (1994). Observations on Experimental, Nonchannelized, High-Concentration Turbidity Currents and Variations in Deposits Around Obstacles. *Jour. Sed. Res.* 64, 899–909. doi:10.1306/d4267f00-2b26-11d7-8648000102c1865d

Allen, P. A., and Underhill, J. R. (1989). Swaley Cross-Stratification Produced by Unidirectional Flows, Bencliff Grit (Upper Jurassic), Dorset, UK. *J. Geol. Soc.* 146, 241–252. doi:10.1144/gsjgs.146.2.0241

Amy, L. A., McCaffrey, W. D., and Kneller, B. C. (2004). "The Influence of a Lateral basin-slope on the Depositional Patterns of Natural and Experimental Turbidity Currents," in *Deep-water Sedimentation in the Alpine Foreland Basin of the SE France: New Perspectives on the Grès d'Annot and Related Systems*. Editors P. Joseph, and S. A. Lomas (Bath, United Kingdom: Geological Society of London, Special Publications), 221, 311–330. doi:10.1144/gsl.sp.2004.221.01.17

Amy, L. A., and Talling, P. J. (2006). Anatomy of Turbidites and Linked Debrites Based on Long Distance (120 X 30 Km) Bed Correlation, Marnoso Arenacea Formation, Northern Apennines, Italy. *Sedimentology* 53, 161–212. doi:10.1111/j.1365-3091.2005.00756.x

Arnott, R. W., and Southard, J. B. (1990). Exploratory Flow-Duct Experiments on Combined-Flow Bed Configurations, and Some Implications for Interpreting Storm-Event Stratification. *Jour. Sed. Petr.* 60, 211–219. doi:10.1306/212f9156-2b24-11d7-8648000102c1865d

Baas, J. H., Best, J. L., and Peakall, J. (2011). Depositional Processes, Bedform Development and Hybrid Bed Formation in Rapidly Decelerated Cohesive (Mud-sand) Sediment Flows. *Sedimentology* 58, 1953–1987. doi:10.1111/j.1365-3091.2011.01247.x

Baas, J. H., Best, J. L., Peakall, J., and Wang, M. (2009). A Phase Diagram for Turbulent, Transitional, and Laminar clay Suspension Flows. *J. Sediment. Res.* 79, 162–183. doi:10.2110/jsr.2009.025

Baas, J. H., Best, J., and Peakall, J. (2021). Rapid Gravity Flow Transformation Revealed in a Single Climbing Ripple. *Geology* 49, 493–497. doi:10.1130/g48181.1

Baker, M. L., and Baas, J. H. (2020). Mixed Sand-Mud Bedforms Produced by Transient Turbulent Flows in the Fringe of Submarine Fans: Indicators of Flow Transformation. *Sedimentology* 67, 2645–2671. doi:10.1111/sed.12714

Baruffini, L., and Papani, L. (2017). An Introduction to the Physical Stratigraphy and Facies of the Upper Cretaceous Helmintoid Flysch, Western Alps and NW Apennine. *33rd Int. Meet. Sedimentology – Tolouse*, 10–12.

Bell, D., Stevenson, C. J., Kane, I. A., Hodgson, D. M., and Poyatos-Moré, M. (2018). Topographic Controls on the Development of Contemporaneous but Contrasting basin-floor Depositional Architectures. *Jour. Sed. Res.* 88, 1166–1189. doi:10.2110/jsr.2018.58

Cartigny, M. J. B., Ventra, D., Postma, G., and Van den Berg, J. H. (2014). Morphodynamics and Sedimentary Structures of Bedforms under Supercritical-Flow Conditions: New Insights from Flume Experiments. *Sedimentology* 61, 712–748. doi:10.1111/sed.12076

Cerone, D., Gallicchio, S., Moretti, M., and Tinterri, R. (2017). Vertical facies evolution of the Tufiti di Tusa Formation cropping out in the Lucanian Apennines (Southern Italy). *Jour. Med. Earth Sci.* 9, 109–112.

Chough, S. K., and Sohn, Y. K. (1990). Depositional Mechanics and Sequences of Base Surges, SongaKsan Tuff Ring, Cheju Island, Korea. *Sedimentology* 37, 1115–1135. doi:10.1111/j.1365-3091.1990.tb01849.x

de Jager, J. (1979). The Relation Between Tectonics and Sedimentation Along the "Sillaro line" (northern Appennines, Italy). *Geol. Ultraiectina*, 19, 97.

Dumas, S., Arnott, R. W. C., and Southard, J. B. (2005). Experiments on Oscillatory-Flow and Combined-Flow Bed Forms: Implications for Interpreting Parts of the Shallow-Marine Sedimentary Record. *J. Sediment. Res.* 75, 501–513. doi:10.2110/jsr.2005.039

Edwards, D. A., Leeder, M. R., Best, J. L., and Pantin, H. M. (1994). On Experimental Reflected Density Currents and the Interpretation of Certain Turbidites. *Sedimentology* 41, 437–461. doi:10.1111/j.1365-3091.1994.tb02005.x

Ellis, D. (1982). *Palaeohydraulics and Computer Simulation of Turbidites in the Marnoso-Arenacea, Northern Apennines, Italy. PhD Thesis*. Scotland: University of St. Andrews.

Fallgatter, C., Kneller, B. C., Paim, P., and Milana, J. P. (2016). Hybrid Megabeds Deposition and the Influence of Related Topography in Ponding Subsequent Co-genetic Flow: Cerro Bola Area, Paganzo Basin, Argentina. *Sedimentology* 64, 357–387.

Fedele, J. J., Hoyal, D. C. J. D., Barnaal, Z., Tulenko, J., and Awalt, S. (2016). "Bedforms Created by Gravity Flows," in *Autogenic Dynamics and Self-Organization in Sedimentary Systems* (Broken Arrow, OK, United States: SEPM Special Publication), 106, 95–121.

Felletti, F., Marini, M., Bellin, N., and Talling, P. (2019). Geometry and Internal Facies Partitioning of the Contessa Megaturbidite from Long Distance (130-30 Km) Correlation (Miocene Marnoso Arenacea Fm; Northern Apennines, Italy). *34th Int. Meet. Sedimentology – Rome*, 10–13.

Fontana, D., Spadafora, E., and Stefani, C. (1994). The Upper Cretaceous Helmintoid Flysch of the Northern Apennines: Provenance and Sedimentation. *Mem. Soc. Geol. It.* 48, 237–250.

Gandolfi, G., Paganelli, L., and Zuffa, G. G. (1983). Petrology and Dispersal Pattern (Miocene, Northern Apennines). *Jour. Sed. Petrol.* 53, 493–507.

Ghienne, J. F., Girard, F., Moreu, J., and Rubino, J. L. (2010). Late Ordovician Climbing-Dune Cross-Stratification: a Signature of Outburst Floods in Proglacial Outwash Environments? *Sedimentology* 57, 1175–1198.

Gladstone, C., McClelland, H. L. O., Woodcock, N. H., Pritchard, D., and Hunt, J. E. (2018). The Formation of Convolute Lamination in Mud-rich Turbidites. *Sedimentology* 65, 1800–1825. doi:10.1111/sed.12447

Hand, B. M., and Bartberger, C. E. (1988). Leeside Sediment Fallout Patterns and the Stability of Angular Bedforms. *Jour. Sed. Petr.* 58, 33–43.

Harms, J. C. (1969). Hydraulic Significance of Some Sand Ripples. *Geol. Soc. America Bull.* 80, 363–396. doi:10.1130/0016-7606(1969)80[363:hsossr]2.0.co;2

Haughton, P. (2001). Contained Turbidites Used to Track Sea Bed Deformation and basin Migration, Sorbas Basin, South-East Spain. *Basin Res.* 13, 117–139. doi:10.1046/j.1365-2117.2001.00143.x

Haughton, P. D. W. (1994). Deposits of Deflected and Ponded Turbidity Currents, Sorbas Basin, Southeast Spain. *J. Sediment. Res.* 64, 233–246. doi:10.1306/d4267d6b-2b26-11d7-8648000102c1865d

Howlett, D. M., Ge, Z., Nemec, W., Gawthorpe, R. L., Rotevatn, A., and Jackson, C. A. L. (2019). Response of Unconfined Turbidity Current to Deep-water Fold and Thrust belt Topography: Orthogonal Incidence on Solitary and Segmented Folds. *Sedimentology* 66, 2425–2454. doi:10.1111/sed.12602

Haughton, P. D. W., Davis, C., McCaffrey, W. D., and Barker, S. (2009). Hybrid sediment gravity flow deposits – classification, origin and significance. *Mar. Petrol. Geology* 26, 1900–1918.

Kane, I. A., McCaffrey, W. D., and Martinsen, O. J. (2009). Allogenic vs. Autogenic Controls on Megaflute Formation. *J. Sediment. Res.* 79, 643–651. doi:10.2110/jsr.2009.072

Kleverlaan, K. (1987). Gordo Megabed: a Possible Seismite in a Tortonian Submarine Fan, Tabernas basin, Province Almeria, Southeast Spain. *Sediment. Geology.* 51, 165–180. doi:10.1016/0037-0738(87)90047-9

Kneller, B. (1995). "Beyond the Turbidite Paradigm: Physical Models for Deposition of Turbidites and Their Implications for Reservoir Prediction," in *Characterization of Deep Marine Clastic Systems, 4*. Editors A. J. Hartlet, and D. J. Prosser (Bath, UK: Geological Society, London, Special Publications), 94, 31–49. doi:10.1144/gsl.sp.1995.094.01.04*Geol. Soc. Lond. Spec. Publications*

Kneller, B. C., and Branney, M. J. (1995). Sustained High-Density Turbidity Currents and the Deposition of Thick Massive Sands. *Sedimentology* 42, 607–616. doi:10.1111/j.1365-3091.1995.tb00395.x

Kneller, B., Edwards, D., McCaffrey, W., and Moore, R. (1991). Oblique Reflection of Turbidity Currents. *Geol* 19, 250–252. doi:10.1130/0091-7613(1991)019<0250:orotc>2.3.co;2

Koller, D., Manica, R., Borges, A. L., and Fedele, J. (2019). Experimental Bedforms by saline Density Currents. *Braz. J. Geology.* 49, 20180118. doi:10.1590/2317-4889201920180118

Labaume, P., Mutti, E., and Seguret, M. (1987). Megaturbidites: A Depositional Model from the Eocene of the SW-Pyrenean Foreland Basin, Spain. *Geo-Marine Lett.* 7, 91–101. doi:10.1007/bf02237988

Labaume, P., Mutti, E., Seguret, M., and Rosell, J. (1983). Megaturbidites carbonatees du bassin turbiditique de l'Eocene inferieur et moyen sud-pyreneen. *Bull. de la Societe Geologique de France* S7-XXV, 927–941. doi:10.2113/gssgfbull.s7-xxv.6.927

Lamb, M. P., Hickson, T., Marr, J. G., Sheets, B., Paola, C., and Parker, G. (2004). Surging versus Continuous Turbidity Currents: Flow Dynamics and Deposits in an Experimental Intraslope Minibasin. *J. Sediment. Res.* 74, 148–155. doi:10.1306/062103740148

Lamb, M. P., and Parsons, J. D. (2005). High-density Suspensions Formed under Waves. *J. Sediment. Res.* 75, 386–397. doi:10.2110/jsr.2005.030

Lowe, D. R., and Guy, M. (2000). Slurry-flow Deposits in the Britannia Formation (Lower Cretaceous), North Sea: a New Perspective on the Turbidity Current and Debris Flow Problem. *Sedimentology* 47, 31–70. doi:10.1046/j.1365-3091.2000.00276.x

Marjanac, T. (1990). Reflected Sediment Gravity Flows and Their Deposits in Flysch of Middle Dalmatia, Yugoslavia. *Sedimentology* 37, 921–929. doi:10.1111/j.1365-3091.1990.tb01834.x

Marroni, M., Meneghini, F., and Pandolfi, L. (2017). A Revised Subduction Inception Model to Explain the Late Cretaceous, Double-Vergent Orogen in the Precollisional Western Tethys: Evidence from the Northern Apennines. *Tectonics* 36, 2227–2249. doi:10.1002/2017tc004627

Marroni, M., Molli, G., Ottria, G., and Pandolfi, L. (2001). Tectono-sedimentary Evolution of the External Liguride Units (Northern Apennines, Italy): Insights in the Pre-collisional History of a Fossil Ocean-Continent Transition Zone. *Geodinamica Acta* 14, 307–320. doi:10.1080/09853111.2001.11432449

Masuda, F., and Yokokawa, M. (1992). Combined Flow Ripples Produced by Flume Experiments. *Sci. Rep. Col. Gen. Educ. Osaka Univ.* 41, 1–13.

McCave, I. N., and Jones, K. P. N. (1988). Deposition of Ungraded Muds from High-Density Non-turbulent Turbidity Currents. *Nature* 333, 250–252. doi:10.1038/333250a0

Mutti, E., Lucchi, F. R., Seguret, M., and Zanzucchi, G. (1984). Seismoturbidites: a New Group of Resedimented Deposits. *Mar. Geology.* 55, 103–116. doi:10.1016/0025-3227(84)90135-x

Mutti, E., Tinterri, R., Benevelli, G., Biase, D. d., and Cavanna, G. (2003). Deltaic, Mixed and Turbidite Sedimentation of Ancient Foreland Basins. *Mar. Pet. Geology.* 20, 733–755. doi:10.1016/j.marpetgeo.2003.09.001

Mutti, E., Tinterri, R., Remacha, E., Mavilla, N., Angella, S., and Fava, L. (1999). *An Introduction to the Analysis of Ancient Turbidite Basins from an Outcrop Perspective*, 39. Tulsa, OK: AAPG Continuing Education Course Notes Series, 93.

Muzzi Magalhaes, P., and Tinterri, R. (2010). Stratigraphy and Depositional Setting of Slurry and Contained (Reflected) Beds in the Marnoso-Arenacea Formation (Langhian-Serravallian) Northern Apennines, Italy. *Sedimentology* 57, 1685–1720. doi:10.1111/j.1365-3091.2010.01160.x

Myrow, P. M., and Southard, J. B. (1991). Combined-flow Model for Vertical Stratification Sequences in Shallow marine Storm Deposited Beds. *Jour. Sed. Petr.* 61, 202–211. doi:10.1306/d42676d1-2b26-11d7-8648000102c1865d

Nøttvedt, A., and Kreisa, R. D. (1987). Model for the Combined-Flow Origin of Hummocky Cross-Stratification. *Geology* 15, 357–361.

Ogata, K., Mutti, E., Pini, G. A., and Tinterri, R. (2012). Mass Transport-Related Stratal Disruption within Sedimentary Mélanges: Examples from the Northern Apennines (Italy) and South-central Pyrenees (Spain). *Tectonophysics* 568-569, 185–199. doi:10.1016/j.tecto.2011.08.021

Pantin, H. M., and Leeder, M. R. (1987). Reverse Flow in Turbidity Currents: the Role of Internal Solitons. *Sedimentology* 34, 1143–1155. doi:10.1111/j.1365-3091.1987.tb00597.x

Parea, G. C., and Ricci Lucchi, F. (1975). Turbidite Key-Beds as Indicators of Ancient Deep-Sea plains. *Proc. IX Int. Cong. Sed., Nice, Theme* 1, 235–245.

Patacci, M., Haughton, P. D. W., and McCaffrey, W. D. (2015). Flow Behavior of Ponded Turbidity Currents. *J. Sediment. Res.* 85, 885–902. doi:10.2110/jsr.2015.59

Patel, U. S., Gardiner, A., and Stow, D. A. V. (2021). Bed-scale Vertical and Lateral Distribution of Massive sandstone in a Topographically Confined basin (Peïra Cava, SE France): Implications for Flow Processes. *Sediment. Geology.* 424, 106001. doi:10.1016/j.sedgeo.2021.106001

Payros, A., Pujalte, V., and Orue-Etxebarria, X. (1999). The South Pyrenean Eocene Carbonate Megabreccias Revisited: New Interpretation Based on Evidence from the Pamplona Basin. *Sediment. Geology.* 125, 165–194. doi:10.1016/s0037-0738(99)00004-4

Piazza, A., and Tinterri, R. (2020). "Mass-Transport Deposits in the Foredeep Basin of the Cervarola Sandstones Formation (Miocene, Northern Apennines, Italy)," in *Submarine Landslides: Subaqueous Mass-Transport Deposits from Outcrops to Seismic Profiles*. Editors K. Ogata, A. Festa, and G. A. Pini Geophysical Monograph 247, First Edition. American Geophysical Union (Hoboken NJ: John Wiley & Sons, Inc.), 27–44.

Pickering, K. T., and Hiscott, R. N. (1985). Contained (Reflected) Turbidity Currents from the Middle Ordovician Cloridorme Formation, Quebec, Canada: an Alternative to the Antidune Hypothesis. *Sedimentology* 32, 373–394. doi:10.1111/j.1365-3091.1985.tb00518.x

Postma, G., and Cartigny, M. J. B. (2014). Supercritical and Subcritical Turbidity Currents and Their Deposits--A Synthesis. *Geology* 42, 987–990. doi:10.1130/g35957.1

Postma, G., Cartigny, M., and Kleverlaan, K. (2009). Structureless, Coarse-Tail Graded Bouma Ta Formed by Internal Hydraulic Jump of the Turbidity Current? *Sediment. Geology.* 219, 1–6. doi:10.1016/j.sedgeo.2009.05.018

Remacha, E., Fernandez, L. P., and Maestro, E. (2005). The Transition between Sheet-like Lobe and basin plain Turbidites in the Hecho basin (Southcentral Pyrenees, Spain). *Jour. Sed. Res.* 75, 789–819. doi:10.2110/jsr.2005.064

Renzi, G. (1964). Un probabile Livello guida nella Formazione Marnoso-arenacea romagnola nei dintorni di Marradi e Palazzuolo. *Quaderni Studi Romagnoli* 1, 15–20.

Ricci Lucchi, F. (1995). Contessa and Associated Megaturbidites: Long Distance (120 × 25 Km) Correlation of Individual Beds in a Miocene Foredeep. *Atlas of Deep Water Environments*, 300–302. doi:10.1007/978-94-011-1234-5_45

Ricci Lucchi, F., and Pialli, G. (1973). Apporti secondari nella Marnoso arenacea: 1. Torbiditi di conoide e di pianura sottomarina ad est-nordest di Perugia. *Bollettino della Società Geologica Italiana* 92, 669–712.

Ricci Lucchi, F. (1985). *Small-scale Antidune Forms on Top of a Megaturbidite sandstone, Northern Apennines*. Lleida, Abs: IAS 5th Regional Meeting, 387–390.

Ricci Lucchi, F. (1986). "The Oligocene to Recent Foreland Basins of the Northern Apennines," in *Foreland Basins, IAS Spec. Publ*. Editors P. A. Allen, and P. Homewood (Oxford: Blackwell Scientific), Vol. 8, 105–139.

Ricci Lucchi, F., and Valmori, E. (1980). Basin-wide Turbidites in a Miocene, Over-supplied Deep-Sea plain: a Geometrical Analysis. *Sedimentology* 27, 241–270. doi:10.1111/j.1365-3091.1980.tb01177.x

Rio, D., and Villa, G. (1987). On the age of the "Salti del Diavolo" conglomerates and of the Monte Cassio Flysch "Basal Complex" (Northern Apennines, Parma province). *Giornale di Geologia* 49 (1), 63–79.

Rupke, N. A. (1976). Sedimentology of Very Thick Calcarenite-Marlstone Beds in a Flysch Succession, Southwestern Pyrenees. *Sedimentology* 23, 43–65. doi:10.1111/j.1365-3091.1976.tb00038.x

Sagri, M., and Marri, C. (1980). Paleobatimetria e ambienti di deposizione delle unità torbiditiche cretaceo-superiori dell'Appennino settentrionale. *Società Geologica Italiana Memorie* 21, 231–240.

Saunderson, H., and Lockett, F. P. J. (1983). "Flume Experiments on Bedforms and Structures at the Dune-Plane Bed Transition," in *Modern and Ancient Fluvial Systems, IAS Spec*. Editors J. D. Collinson, and J. Lewin (Blackwell: Publ.), 6, 49–58.

Schieber, J., and Southard, J. B. (2009). Bedload Transport of Mud by Floccule Ripples-Direct Observation of Ripple Migration Processes and Their Implications. *Geology* 37, 483–486. doi:10.1130/g25319a.1

Schieber, J., Southard, J., and Thaisen, K. (2007). Accretion of Mudstone Beds from Migrating Floccule Ripples. *Science* 318, 1760–1763. doi:10.1126/science.1147001

Scholle, P. A. (1971). Sedimentology of fine-grained Deep-Water Carbonate Turbidites, Monte Antola Flysch (Upper Cretaceous), Northern Apennines, Italy. *Geol. Soc. America Bull.* 82, 629–658. doi:10.1130/0016-7606(1971)82[629:sofdct]2.0.co;2

Soutter, E. L., Bell, D., Cumberpatch, Z. A., Ferguson, R. A., Spychala, Y. T., Kane, I. A., et al. (2021). The Influence of Confining Topography Orientation on Experimental Turbidity Currents and Geological Implications. *Front. Earth Sci.* 8, 540633. doi:10.3389/feart.2020.540633

Stevenson, C. J., Talling, P. J., Masson, D. G., Sumner, E. J., Frenz, M., and Wynn, R. B. (2014). The Spatial and Temporal Distribution of Grain-Size Breaks in Turbidites. *Sedimentology* 61, 1120–1156. doi:10.1111/sed.12091

Sumner, E. J., Talling, P. J., and Amy, L. A. (2009). Deposits of Flows Transitional between Turbidity Current and Debris Flow. *Geology* 37, 991–994. doi:10.1130/g30059a.1

Tagliaferri, A., and Tinterri, R. (2016). The Tectonically-Confined Firenzuola Turbidite System (Marnoso-Arenacea Formation, Northern Apennines, Italy). *It. Jour. Geoscience* 135, 425–443. doi:10.3301/ijg.2015.27

Tagliaferri, A., Tinterri, R., Pontiggia, M., Da Pra, A., Davoli, G., and Bonamini, E. (2018). Basin-scale, High-Resolution Three-Dimensional Facies Modeling of Tectonically Confined Turbidites: An Example from the Firenzuola System (Marnoso-Arenacea Formation, Northern Apennines, Italy). *AAPG Bulletin* 102, 1601–1626. doi:10.1306/12081716521

Talling, P. J., Amy, L. A., Wynn, R. B., Peakall, J., and Robinson, M. (2004). Beds Comprising Debrite Sandwiched within Co-genetic Turbidite: Origin and Widespread Occurrence in Distal Depositional Environments. *Sedimentology* 51, 163–194. doi:10.1111/j.1365-3091.2004.00617.x

Talling, P. J., Masson, D. G., Sumner, E. J., and Malgesini, G. (2012). Subaqueous Sediment Density Flows: Depositional Processes and deposit Types. *Sedimentology* 59, 1937–2003. doi:10.1111/j.1365-3091.2012.01353.x

Tinterri, R., Civa, A., Laporta, M., and Piazza, A. (2020). "Turbidites and Turbidity Currents," in *Regional Geology and Tectonics: Principles of Geologic Analysis*. Editors N. Scarselli, A. Jűrgen, D. Chiarella, D. G. Roberts, and A. W. Bally. 2nd ed. (Elsevier), 1, 441–479.

Tinterri, R. (2011). Combined Flow Sedimentary Structures and the Genetic Link between Sigmoidal and Hummocky-Cross Stratification. *GeoActa* 10, 43–85.

Tinterri, R., and Mazza, T. (2019). Contained-reflected Beds: Examples from Foredeep Turbidites and Helminthoid Flysches of the Northern Apennines (Italy). *34th Int. Meet. Sedimentology – Rome* 10-13, 1879.

Tinterri, R., Muzzi Magalhaes, P., Piazza, A., and Tagliaferri, A. (2019a). Comparing Two Foredeeps: Cervarola Sandstones and Marnoso-Arenacea Formations (Miocene, Northern Apennines, Italy). *34th Int. Meet. Sedimentology – Rome* 10-13, 1601.

Tinterri, R., and Muzzi Magalhaes, P. (2011). Synsedimentary Structural Control on Foredeep Turbidites: an Example from Miocene Marnoso-Arenacea Formation, Northern Apennines, Italy. *Mar. Pet. Geology.* 28, 629–657. doi:10.1016/j.marpetgeo.2010.07.007

Tinterri, R., Muzzi Magalhaes, P., Tagliaferri, A., and Cunha, R. S. (2016). Convolute Laminations and Load Structures in Turbidites as Indicators of Flow Reflections and Decelerations against Bounding Slopes. Examples from the Marnoso-Arenacea Formation (Northern Italy) and Annot Sandstones (South Eastern France). *Sediment. Geology.* 344, 382–407. doi:10.1016/j.sedgeo.2016.01.023

Tinterri, R., Muzzi Magalhaes, P., Tagliaferri, A., and Piazza, A. (2019b). *Foredeep Turbidites of the Marnoso-Arenacea Formation.* In Field Trips Guide book, 34th IAS Meeting, Rome 10-13 september 2019. (Italy; northern Apennines), 323–339.

Tinterri, R., and Muzzi Magalhaes, P. (2009). "The Miocene Turbidite Deposits of the Marnoso-Arenacea Formation (Northern Apennines, Italy)," in *Field Trips Guidebook. 249-277, 27th IAS Meeting of Sedimentology, Alghero 20-23 September 2009, Post Congress Field Trip*. Editors V. Pascucci and S. Andreucci, 12, 24–28.

Tinterri, R., and Piazza, A. (2019). Turbidites Facies Response to the Morphological Confinement of a Foredeep (Cervarola Sandstones Formation, Miocene, Northern Apennines, Italy). *Sedimentology* 66, 636–674. doi:10.1111/sed.12501

Tinterri, R., and Tagliaferri, A. (2015). The Syntectonic Evolution of Foredeep Turbidites Related to basin Segmentation: Facies Response to the Increase in Tectonic Confinement (Marnoso-Arenacea Formation, Miocene, Northern Apennines, Italy). *Mar. Pet. Geology.* 67, 81–110. doi:10.1016/j.marpetgeo.2015.04.006

Tinterri, R., Muzzi Magalhaes, P., and Tagliaferri, A. (2012). Foredeep turbidites of the Miocene Marnoso-arenacea Formation (Northern Apennines). *AAPG International Conference & Exhibition-Milan, Geological Field Trips* 4, 1–132. doi:10.3301/GFT.2012.03

Toniolo, H., Lamb, M., and Parker, G. (2006). Depositional Turbidity Currents in Diapiric Minibasins on the continental Slope: Formulation and Theory. *Jour. Sed. Res.* 76, 783–797. doi:10.2110/jsr.2006.071

Vescovi, P., Fornaciari, E., Rio, D., and Valloni, R. (1999). The Basal Complex Stratigraphy of the Helmintoid Monte Cassio Flysch: a Key to the Eoalpine Tectonics of the Northern Apennines. *Rivista Italiana di Paleontoliga e Stratigrafia* 105, 101–128. doi:10.13130/2039-4942/5367

Woods, A. D., Bursik, M. I., and Kurbatov, A. V. (1998). The Interaction of Ash Flows with Ridges. *Bull. Volcanology.* 60, 38–51.

Yokokawa, M. (1995). Combined Flow Ripples: Genetic Experiments and Application for Geologic Records. Kyushu University, Faculty of Science. *Mem. Ser. D, Earth Planet. Sci.* 29, 1–38.

Yokokawa, M., Masuda, F., and Endo, N. (1995). Sand Particle Movement on Migrating Combined-Flow Ripples. *Jour. Sed. Res.* A65, 40–44.

Zuffa, G. G., Fontana, D., Morlotti, E., Premoli, S. I., Sighinolfi, G. P., Stefani, C., et al. (2004). *Anatomy of Carbonate Turbidite Mega-Beds (M. Cassio Formation, Upper Cretaceous, Northern Apennines*, LXI. Italy: Mem. Descr. Carta Geol. It., 129–144.

Conflict of Interest: Author PM was employed by the company Petrobras.

The remaining authors declare that the research was conducted in the absence of any commercial or financial relationships that could be construed as a potential conflict of interest.

Publisher's Note: All claims expressed in this article are solely those of the authors and do not necessarily represent those of their affiliated organizations, or those of the publisher, the editors and the reviewers. Any product that may be evaluated in this article, or claim that may be made by its manufacturer, is not guaranteed or endorsed by the publisher.